THE GEOLOGICAL SOCIETY OF AMERICA®

An analysis of the factors that control fault zone architecture and the importance of fault orientation relative to regional stress

John M. Fletcher[1,†], Orlando J. Teran[1,§], Thomas K. Rockwell[2], Michael E. Oskin[3], Kenneth W. Hudnut[4], Ronald M. Spelz[5], Pierre Lacan[6], Matthew T. Dorsey[2,#], Giles Ostermeijer[7], Thomas M. Mitchell[7], Sinan O. Akciz[8], Ana Paula Hernandez-Flores[1], Alejandro Hinojosa-Corona[1], Ivan Peña-Villa[1], and David K. Lynch[4]

[1]*Departamento de Geologia, Centro de Investigacion Cientifica y de Educacion Superior de Ensenada, Carretera Tijuana-Ensenada No. 3918, Zona Playitas, Ensenada, Baja California 22860, México*

[2]*Department of Geological Sciences, San Diego State University, 5500 Campanile Drive, San Diego, California 92182, USA*

[3]*Department of Earth and Planetary Sciences, University of California Davis, One Shields Avenue, Davis, California 95616-8605, USA*

[4]*U.S. Geological Survey, 525 & 535 S. Wilson Street, Pasadena, California 91106-3212, USA*

[5]*Universidad Autónoma de Baja California, Facultad de Ciencias Marinas, Carretera Tijuana-Ensenada No. 3917, Zona Playitas, Ensenada, Baja California 22860, México*

[6]*Centro de Geociencias, Universidad Nacional Autónoma de México, Blvd. Juriquilla, 3001, 76230, Juriquilla, Querétaro, México*

[7]*Earth Sciences, University College London, Gower Street, London, WC1E 6BT, UK*

[8]*Geological Sciences, McCarthy Hall 341B, California State University Fullerton, Fullerton, California 92831, USA*

ABSTRACT

The moment magnitude 7.2 El Mayor–Cucapah (EMC) earthquake of 2010 in northern Baja California, Mexico produced a cascading rupture that propagated through a geometrically diverse network of intersecting faults. These faults have been exhumed from depths of 6–10 km since the late Miocene based on low-temperature thermochronology, synkinematic alteration, and deformational fabrics. Coseismic slip of 1–6 m of the EMC event was accommodated by fault zones that displayed the full spectrum of architectural styles, from simple narrow fault zones (<100 m in width) that have a single high-strain core, to complex wide fault zones (>100 m in width) that have multiple anastomosing high-strain cores. As fault zone complexity and width increase the full spectrum of observed widths (20–200 m), coseismic slip becomes more broadly distributed on a greater number of scarps that form wider arrays. Thus, the infinitesimal slip of the surface rupture of a single earthquake strongly replicates many of the fabric elements that were developed during the long-term history of slip on the faults at deeper levels of the seismogenic crust. We find that factors such as protolith, normal stress, and displacement, which control gouge production in laboratory experiments, also affect the architectural complexity of natural faults. Fault zones developed in phyllosilicate-rich metasedimentary gneiss are generally wider and more complex than those developed in quartzo-feldspathic granitoid rocks. We hypothesize that the overall weakness and low strength contrast of faults developed in phyllosilicate rich host rocks leads to strain hardening and formation of broad, multi-stranded fault zones. Fault orientation also strongly affects fault zone complexity, which we find to increase with decreasing fault dip. We attribute this to the higher resolved normal stresses on gently dipping faults assuming a uniform stress field compatible with this extensional tectonic setting. The conditions that permit slip on misoriented surfaces with high normal stress should also produce failure of more optimally oriented slip systems in the fault zone, promoting complex branching and development of multiple high-strain cores. Overall, we find that fault zone architecture need not be strongly affected by differences in the amount of cumulative slip and instead is more strongly controlled by protolith and relative normal stress.

INTRODUCTION

Most faults are characterized by a zone of penetrative fracturing that increases in intensity toward progressively higher strain portions of the fault zone, culminating in a zone of gouge or cataclasite that is recognized as the fault core (e.g., Chester and Logan, 1986; Caine et al., 1996). The thickness of the damage zones of penetrative fracturing (tens to hundreds of meters) is up to several orders of magnitude greater than the width of high-strain fault cores, which generally ranges from a few centimeters to several meters (e.g., Shipton and Cowie, 2001). The internal structure or architecture of a fault zone is defined by the number and distribution of high-strain cores, the overall width and intensity of fracturing in the zone of damage that extends into the country rock, and the presence of subsidiary faults that cut through and, in some cases, extend beyond the limits of the main fault zone (e.g., Faulkner et al., 2010).

A central goal in the study of fault mechanics is to understand how the internal structure of a fault zone relates to its mechanical and seismogenic behavior (Biegel and Sammis, 2004; Frost et al., 2009). The internal structure of a fault zone is recognized to be affected by displacement (e.g., Scholz, 1987; Shipton and Cowie, 2001), lithology (e.g., Faulkner et al., 2003, 2008), preexisting fabric (e.g., Collettini and Sibson, 2001), and depth, the latter of which controls gradients in temperature, confining pressure, and fluid pressure (e.g., Sibson, 1977; Butler et al., 1995; Wibberley et al., 2008). Interseismic healing may significantly change the mechanical behavior of a fault and is thought to occur due to post-seismic compaction and lithification of fractured fault rocks (e.g., Karner et al., 1997). Understanding the complex interplay between all of these variables requires the integration

[†]jfletche@cicese.mx.

[§]Present address: Ovintiv, The Woodlands, Texas 77380, USA.

[#]Present address: Department of Geology and Geophysics, Texas A&M University, College Station, Texas 77843, USA.

GSA Bulletin; September/October 2020; v. 132; no. 9/10; p. 2084–2104; https://doi.org/10.1130/B35308.1; 14 figures; 2 tables.
published online 6 March 2020

of results from laboratory experiments and mechanical modeling, with direct observations of the faults themselves from structural and seismological studies.

The internal structure, or architecture, of a fault zone not only reflects its physical properties but also its mechanical evolution and mode of slip. Faulkner et al. (2003, 2010) described fault zones with two contrasting architectural styles. The first is a simple fault zone with a single high-strain core. Many workers recognize a positive feedback between slip and various transformation weakening processes associated with cataclasis (e.g., Chester et al., 1993; Yan et al., 2001). Progressive strain softening is thought to cause fault zones to evolve toward architectural simplicity with shear concentrated into a single, narrow core that lies within the variably fractured damage zone (e.g., Chester et al., 1993; Ben-Zion and Sammis, 2003; Cowgill et al., 2004a; Rockwell and Ben Zion, 2007; Frost et al., 2009). Because slip localization is required for seismic rupture nucleation and propagation, the mode of displacement accommodated by single-cored faults is thought to be dominated by stick-slip (Chester and Logan, 1986). However, this model of fault zone evolution cannot explain the occurrence of complex fault zones that are much wider and have multiple overlapping high-strain cores, which constitute the second architectural style described by Faulkner et al. (2003). The evolution of a fault zone toward structural complexity is hypothesized to result from strain hardening, which causes slip to relocate and leads to the development of multiple overlapping high-strain cores (Faulkner et al., 2003, 2008; Cowgill et al., 2004a). The Carboneras fault of Spain and the Parkfield section of the San Andreas fault in California, USA, are two well studied examples of wide multi-core fault zones (Rymer et al., 2006; Bradbury et al., 2011). Both are hosted within weak phyllosilicate-rich country rock and demonstrate mixed-mode displacement with stable creep associated with large numbers of small earthquakes interpreted to represent localized patches of the fault surface undergoing stick slip sliding surrounded by stable sliding areas (Rubin et al., 1999; Faulkner et al., 2003).

The Sierra Cucapah in northern Baja California, Mexico is an ideal natural laboratory for testing hypothesized controls on fault zone architecture. It is located near the axis of shearing between the Pacific and North American plates and contains a diverse array of faults that accommodate three dimensional, transtensional strain. Individual faults have large variations in cumulative slip, protolith, and kinematics, which allow us to assess the role of each of these parameters in generating fault zones with a spectrum of architectural styles. Importantly, all of the faults in the Sierra Cucapah are active and many have segments that slipped in the 2010 moment magnitude (M_W) 7.2 El Mayor–Cucapah (EMC) earthquake (Fletcher et al., 2014). This study builds on the work of Teran et al. (2015) to document how fault-zone architecture evolves with the coseismic slip, and, in turn, how this architecture affects rupture propagation. We provide field evidence demonstrating that the architecture of a fault is strongly affected by its orientation relative to regional principal stresses. We find that as the slip tendency or ratio of shear to normal stress (Morris et al., 1996; Tong and Yin, 2011) on a fault decreases, its width and architectural complexity increases. Overall, we show that factors known to increase gouge production in the laboratory setting, such as protolith rheology, normal stress, and cumulative slip (e.g., Yoshioka, 1986), also increase the width and architectural complexity of natural faults.

GENERAL GEOLOGY OF THE SIERRA CUCAPAH

The Sierra Cucapah forms an uplifted massif of crystalline basement that rises 1 km in relief above the surrounding rift valley floor (Fig. 1). Plate margin faults are exceptionally well exposed in this remote desert region of northern Baja California and have been exhumed from depths of 6–10 km since the late Miocene (Axen et al., 2000), which corresponds to the middle to lower portion of the seismogenic crust. The faults have a wide range of orientations, and individual fault sections vary in strike from 290° to 040° with dips that vary from 90° to 20° (Fletcher et al., 2014; Teran et al., 2015). In map view, the faults are short (20–30 km), discontinuous and end at intersections with other faults (Fig. 2). In three dimensions this fault system forms a complex interlocking network, which gives rise to intimate mechanical interactions between faults (Fletcher et al., 2016). The M_W 7.2 EMC earthquake of 2010 demonstrated that the complex fault network failed as an integrated system and its strength was controlled by the cross-cutting misoriented faults that support higher levels of shear stress (Fletcher et al., 2016).

The geometric diversity of faults in the complex network gives rise to kinematic diversity. Shear sense varies from pure normal dip slip to pure dextral strike slip, but most faults have oblique slip defined by some combination of normal and lateral shear (Fletcher et al., 2014). Although highly variable, slip direction is not random. Fletcher et al. (2016) demonstrated that incremental changes in fault orientation are associated with incremental changes in the rake of slip. Moreover, they showed that coseismic slip directions are consistent with the variations predicted by uniform regional stress state (e.g., Wallace, 1951; Bott, 1959) where the maximum principal stress is vertical, the minimum is horizontal trending ENE, and the intermediate principal stress is close in magnitude to the maximum and trends NNW. This stress state is consistent with prolate triaxial strain, which is expected in a transtensional shear zone (e.g., Fossen et al., 1994). Therefore, the complexity of faulting in the Sierra Cucapah, with all of its diversity, is required to accommodate the three-dimensional strain of this transtensional plate margin.

The crystalline basement of the Sierra Cucapah is a lithologically diverse sequence of metamorphic and plutonic rocks of Jurassic and Cretaceous age (Barnard, 1968; Axen et al., 2000). Surrounding the Sierra Cucapah, these rocks are juxtaposed by faults against synrift sedimentary sequences that reach 4 km in thickness (Kelm, 1971; García-Abdeslem et al., 2001; Fletcher and Spelz, 2009; Chanes-Martínez et al., 2014) and range in age from late Miocene to the present (Seim, 1992; Dorsey and Martin-Barajas, 1999; Chanes-Martínez et al., 2014; Fig. 2). The central portion of the range contains a dismembered, compositionally zoned batholith of Late Cretaceous age (Barnard, 1968). The batholith has a felsic core of unfoliated to weakly foliated granodiorite (Cucapah granodiorite) that intrudes a more mafic but compositionally heterogeneous complex of strongly foliated metaigneous gneiss (La Puerta tonalite in Fig. 2). Along the outer intrusive contact of the granodioritic core, Barnard (1968) mapped a foliated rock unit of intermediate composition that he termed the melanocratic intrusive phase. This rock unit pinches and swells along strike and in places reaches as much as 2 km in thickness. The northern third of the Sierra Cucapah along with much of Sierra El Mayor immediately to the south are dominated by an extensive sequence of upper amphibolite facies metasedimentary gneiss (green unit in Fig. 2; Barnard, 1968). Abundant cross-cutting intrusive contacts and systematic variations in the thickness of ductility deformed rock units provide abundant markers that act as piercing points to determine cumulative offset across individual faults. Below we summarize the geometry, cross cutting relations and cumulative offset of the main faults examined in this study.

Cumulative Offset

The Laguna Salada fault defines the western limit of the Sierra Cucapah and controls a sharp linear mountain front juxtaposed against the northern half of the Laguna Salada Basin (Fig. 1; Barnard, 1968; Chora-Salvador, 2003; Mueller

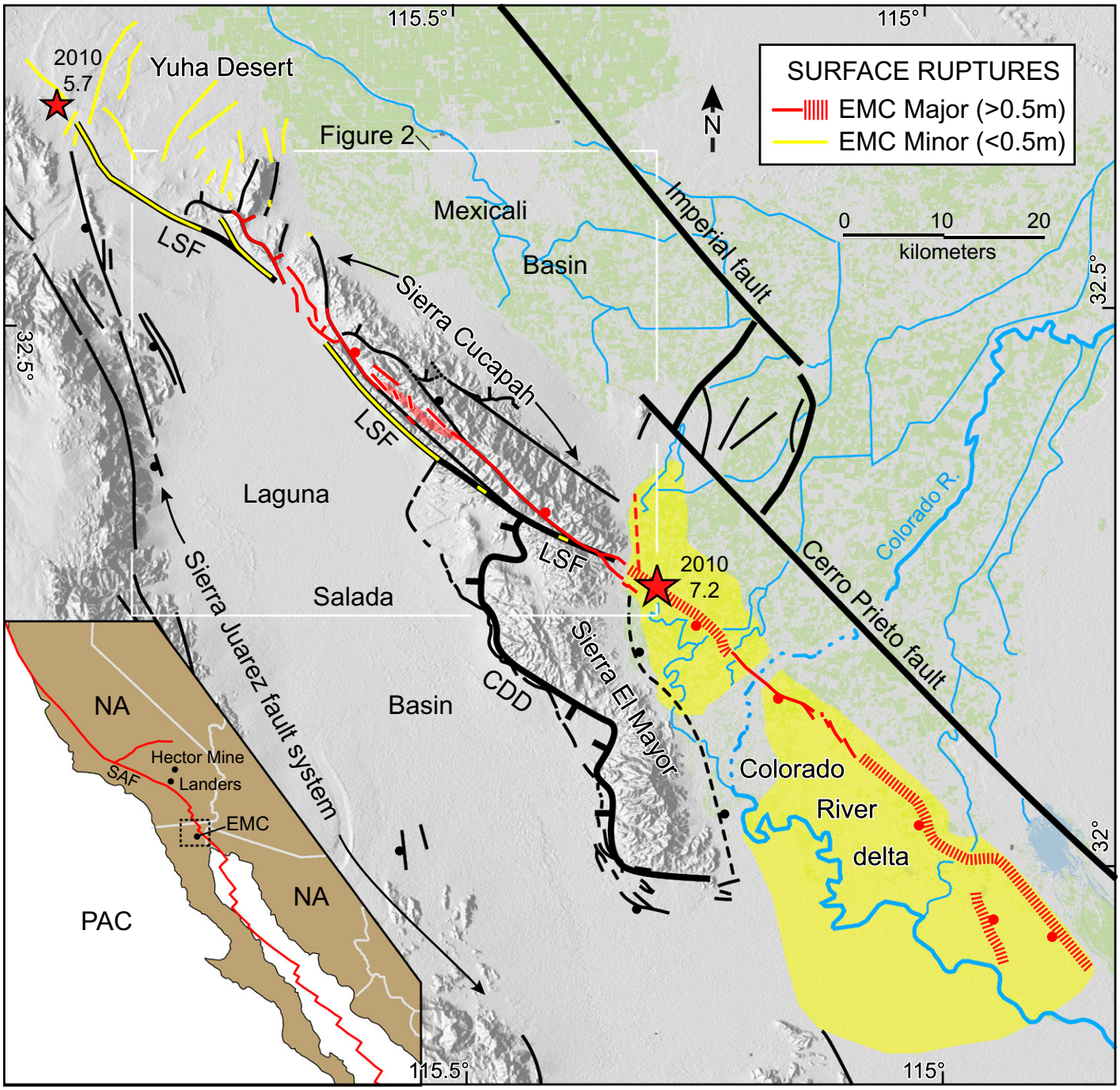

Figure 1. Seismotectonic map of northern Baja California, Mexico, showing the dominant faults (thick black lines) along this part of the plate margin (see inset map). The 2010 El Mayor–Cucapah (EMC) epicenter is shown as the red star and its surface rupture in red and yellow lines. Red hachured line ornament represents distributed coseismic surface flexure above the blind Indiviso fault. Solid circle ornamentation shows down dropped hanging wall of each fault. In the Colorado River delta region, yellow envelopes delimit the approximate extent of 2010 EMC liquefaction-induced ground failure. In the delta, laterally continuous surface displacements were only observed from synthetic aperture radar interferometry (Wei et al., 2010; Oskin et al., 2012) and differential light detection and ranging (Oskin et al., 2012) and are respectively shown as thick hachured lines and solid lines. Labels include: LSF—Laguna Salada fault; CDD—Cañada David detachment. Inset map of the Pacific–North American plate margin also shows epicentral locations of the 2010 EMC event, 1999 Hector Mine and 1992 Landers, all of which produced complex multifault ruptures. Figure modified from Fletcher et al. (2014). Dashed line north of EMC epicenter marks location of normal fault in subsurface, on which the earthquake initiated. Abbreviations in inset map denote the North American (NA) and Pacific (PAC) plates and San Andreas fault (SAF).

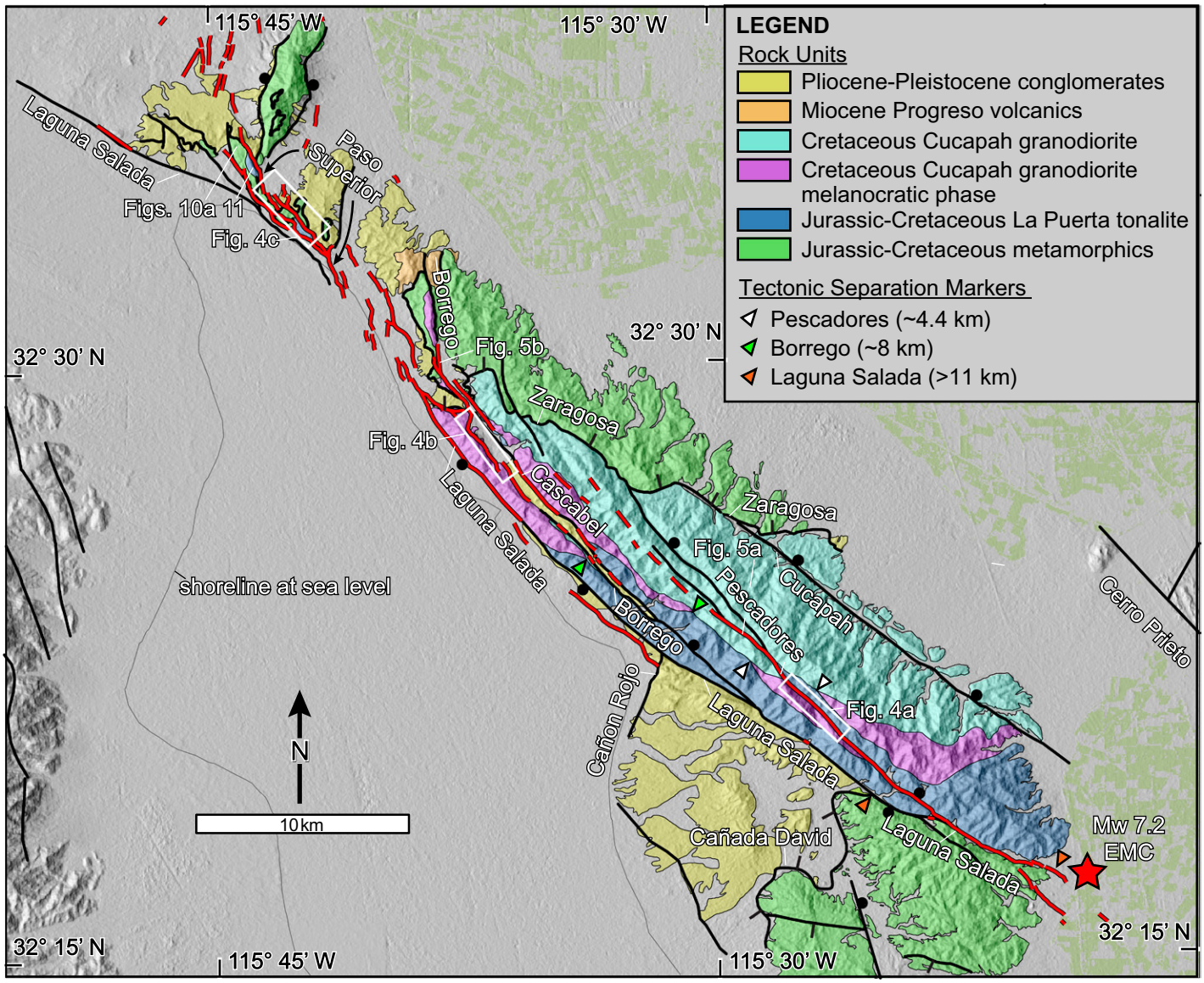

Figure 2. Simplified geologic map of the Sierra Cucapah, northern Baja California, Mexico, showing the main rock packages and faults mapped by Barnard (1968), Chora-Salvador (2003), and from this study. Black lines represent all faults; hanging wall indicated by tick marks for detachment faults and round symbols for steeper faults. Pinchouts of the melanocratic phase of the Cucapah granodiorite defines subvertical piercing points, which are offset by both the Borrego and Pescadores faults for a total of ~6–8 and ~4.4 km, respectively. Along-strike lithologic mismatch across the Laguna Salada fault (red triangles) requires a minimum of ~11 km of dextral offset. Cumulative offset on the Laguna Salada fault must increase north of its intersection with the Cañada David detachment, which accommodates an additional 14 km of west directed transport (Fletcher and Spelz, 2009). White rectangles delineate detailed maps shown in Figure 4. Red star marks the epicenter of the 2010 El Mayor–Cucapah (EMC) earthquake and the segments of faults activated in this event are shown in red.

and Rockwell, 1991, 1995; Axen and Fletcher, 1998; Fletcher and Spelz, 2009). Basin fill along the Laguna Salada fault reaches 3–4 km in thickness based on gravimetric modeling (Kelm, 1971; García-Abdeslem et al., 2001; Fletcher and Spelz, 2009). At the junction of the Sierra Cucapah with the Sierra El Mayor, the west-directed Cañada David detachment transfers 14 km of horizontal displacement (Fletcher and Spelz, 2009) onto the Laguna Salada fault (Fig. 2). Along its southern mapped extent, the Laguna Salada fault places prebatholithic metasedimentary rocks of the Sierra El Mayor against the plutonic rocks of the Sierra Cucapah (Fig. 2). The fact that these rocks have a similar unroofing history (Axen et al., 1998) indicates little vertical motion across the Laguna Salada fault here. Thus its cumulative right lateral slip must be >11 km, which is the length of exposed fault contact between dissimilar basement rocks.

The Pescadores fault splays off the Laguna Salada fault and extends toward the north along the western side of the Sierra Cucapah crest (Fig. 2; Barnard, 1968). In general, the Pescadores fault is subplanar, strikes ~310°, and dips steeply (~75°) to the northeast. The Borrego fault is another splay that extends toward the north from the Laguna Salada fault (Fig. 2). Its curvilinear mapped trace spans a wide range of dips (40°–84°) toward the northeast (Barnard, 1968;

Fletcher et al., 2014). Cumulative offset on both faults may be constrained from offset of piercing lines formed by the sub-vertical pinch-out of the melanocratic phase of the Cretaceous Cucapah igneous complex (Fig. 2). We recognize ~4.4 km of dextral-normal slip on the Pescadores fault, and 6–8 km dextral-normal slip on the Borrego fault. Near its northern limit, the Pescadores fault bifurcates and is cut by the Zaragosa detachment (Fig. 2), whereas the Borrego fault cuts off this detachment. The immediate hanging wall of the Borrego fault consists of late Tertiary rift basin sediments that likely represent a dismembered sliver captured from the paleomargin of the Laguna Salada basin (Fig. 2).

The Paso Superior detachment dips as low as 20° and has a curviplanar surface defined by several prominent megamullions (Fig. 2; Fletcher et al., 2014). Two prominent ramp sections are observed where dip increases to 40°–55° (Fletcher et al., 2014). The fault controls an extensive sedimentary basin that is 3–5 km in width. The vertical component of cumulative offset across the Paso Superior detachment is estimated to be at least 5–6 km, which is a minimum amount of tectonic exhumation since the late Miocene as documented with thermochronology on other detachment faults in the area that have similar structural relations (Axen et al., 2000). The cumulative slip on the Paso Superior detachment is likely to be two to three times greater than the vertical unroofing due to both the shallow dip of the fault and the strong component of right-lateral slip that it accommodates.

Fault Zone Architecture

Fault zone architecture represents the internal configuration of structures and fabrics produced by shearing and is defined in terms of three main rock units: unfractured protolith, damage zone, and fault core (e.g., Chester and Logan, 1986; Caine et al., 1996). Most slip occurs in the fault core, which is composed of a wide range of high-strain fault rocks including breccia, gouge, cataclasites, and ultracataclasites (Mitchell and Faulkner, 2009, and references therein). Fault zones can have multiple cores, with more cores reflecting more complexity (Faulkner et al., 2003, 2008; Mitchell and Faulkner, 2009), although not all fault cores need to have slipped simultaneously. The damage zone is the heavily fractured rock that surrounds the core(s). The degree of damage may be measured by the density of fractures and/or healed fluid inclusion planes, which typically diminish exponentially with distance from a fault core and eventually grades into the background fracture density of the surrounding protolith host rock (Chester and Logan, 1986; Mitchell and Faulkner, 2009; Rockwell et al., 2009; Rempe et al., 2013 Morton et al., 2012). Another important structural element of fault zone architecture are subsidiary faults, which have focused shear strain that is greater than that of rocks in the damage zone, but significantly less than that observed in the fault cores. Subsidiary faults may either branch from the fault cores or cut them. Additionally, they can exist entirely within the damage zone or extend beyond the fault zone and into the surrounding protolith.

In this paper we utilize the work of Teran et al. (2015) who presented systematic mapping at scales of 1:500 or better for all the fault sections that ruptured in the 2010 M_W 7.2 EMC earthquake. The identification of the outer limits of the fault zones was aided by a strong contrast in outcrop weathering resistance between highly fractured fault rocks and crystalline basement with a background intensity of fractures (Teran et al., 2015).

Rupture Zone Fabric

Rupture zone fabric is a general term we use to describe the distribution and internal configuration of coseismic slip, as revealed by fault-scarp arrays cutting the ground surface. Some of its defining characteristics include: (1) rupture zone thickness, (2) number of scarps, (3) distribution and partitioning of coseismic slip across scarps within the rupture zone, (4) existence of a principal displacement scarp, and (5) geometric arrangement of different sets of scarps, patterns of splaying, and degree of interconnectivity (Teran et al., 2015). Based on these characteristics, Teran et al. (2015) developed a set of parameters that could be systematically and quantitatively documented along the length of the 2010 EMC surface rupture in the Sierra Cucapah. They found that rupture zone thickness varies by more than an order of magnitude (12–262 m), and as rupture zone thickness increases, so does the number of coseismic scarps counted in strike-perpendicular transects. Therefore, this suggests that as rupture zones become wider, coseismic slip becomes more broadly distributed on multiple scarps in progressively more complex arrays.

Coseismic slip partitioning is expressed in terms of variations in the magnitude and sense of offset accommodated by individual members of a fault scarp array, and both of these kinematic parameters were systematically compiled by Fletcher et al. (2014). Teran et al. (2015) classified all scarps of the 2010 EMC rupture in the Sierra Cucapah into four categories based on relative magnitude of the total coseismic slip that the principal scarp accommodates in any given strike perpendicular transect: >90%, 60%–90%, 30%–60%, <30%. We show that this classification scheme can be used to distinguish fault sections with slip that is focused onto a single principal scarp that accommodates most of the coseismic slip from those with more broadly distributed slip on multiple overlapping scarps. Coseismic slip partitioning among individual faults of a scarp array is also key for defining the symmetry of coseismic slip distribution relative to important structural elements such as the principal fault scarp, the tectonic contact separating distinct fault blocks, and the boundaries of the long-lived master fault zone.

CASE STUDIES

In this paper, we build on the work of Teran et al. (2015) who showed that rupture zone thickness is strongly correlated with the thickness of the damage zone of the fault along which it propagated (Fig. 3). These relationships strongly suggest that many important aspects of rupture zone fabric are related to the architecture of the long-lived fault zone. This raises questions concerning whether one phenomenon controls the other or if some other processes related to seismogenic failure may drive development of both rupture zone fabric and fault zone architecture.

In order to understand the factors and processes that control rupture zone fabric and its relationship with the structural evolution of the host fault zone, we mapped three case studies in detail. Each contains an association of multiple characteristics that represent important categories that define distinct levels in a spectrum of increasing variations in structural complexity. The architectural complexity of a long-lived fault zone is represented by increasing width, number of cores, and the role of subsidiary faults. The complexity of fracture fabrics formed in the rupture zone of an infinitesimal increment of coseismic slip is represented by increasing width, number of scarps, kinematic partitioning, and role of subsidiary faults. These and other key geometric, kinematic, and lithologic characteristics are described in detail below and summarized in Table 1.

Type 1: Narrow Fault Zones with Highly Focused Strain

The Pescadores fault has one of the narrowest and structurally simplest fault zones in the Sierra Cucapah (Figs. 4A, 5A, and 6). It dips steeply (~75°) and has a relatively straight trace through the high-relief mountainous terrain along the crest of the Sierra Cucapah (Fig. 4A). Its fault zone is ~20 m wide and is dominantly composed of unconsolidated fault breccia and gouge developed in the granitoid rocks that comprise both the footwall and hanging wall (Fig. 6). More resistant

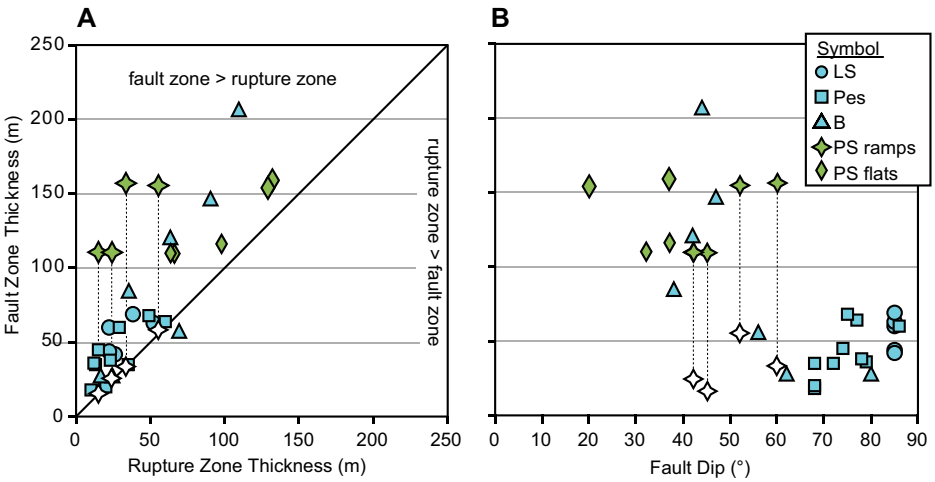

Figure 3. Scatter plots showing variations of fault zone thickness with (A) rupture zone thickness and (B) fault dip from faults in the Sierra Cucapah, Baja California, Mexico. The thickness of the zone of coseismic surface rupture is strongly correlated with the thickness of the fault zone but in general is not as wide. Both of these structural parameters increase as fault dip shallows. Vertical dashed lines connect symbols of the long lived Paso Superior fault zone (green filled) with symbols of the subsidiary cross cutting ramp (white filled). Fault abbreviations include: B—Borrego; LS—Laguna Salada; PS—Paso Superior; Pes—Pescadores. Figure modified from Teran et al. (2015).

outcrops of the host rock prominently define the outer margins of the fault zone (Fig. 6). The fault core contains foliated clay gouge (<1 m thick) that has likely accommodated most of the cumulative geologic slip of ~4.4 km. The core coincides with the trace of paleo-bedrock fault scarps and contains the principal displacement scarp of the 2010 EMC rupture (Fig. 6).

The EMC rupture associated with the Pescadores fault extends ~15 km along strike and generally consists of a single, prominent principal scarp from which emanate a series of secondary fractures with a Riedel-like obliquity (Figs. 4A and 6A). Total coseismic slip is strongly oblique with an average ~2.5 m of dextral and ~0.9 m normal slip (Fletcher et al., 2014). A principal scarp with >90% of total coseismic slip dominates the northern 10 km of this rupture section (Fig. 4A). In the south, near the intersection with the Laguna Salada fault, where the rupture branched from one master fault to another (Fig. 2), the relative displacement on the principal scarp decreases to 60%–90% and coseismic slip is somewhat more distributed. Although the Pescadores fault has a highly linear trace, the principal scarp is not continuous along strike, but rather is divided into segments that are generally <3 km in length and separated by discontinuities that occur as short en echelon steps (100–150 m wide). Secondary fault scarps are generally much shorter in length (<120 m). They typically splay obliquely from the principal scarp and extend to the lateral limit of the damage zone where they curve into parallelism with the principal scarp. In general, the rupture zone does not exceed 20 m in thickness, which coincides with the width of the fault zone. However, Teran et al. (2015) documented short anomalously wide sections with thicknesses as great as ~60 m. These wider sections, extending several hundred meters along strike, may be related to step-overs between spatially distinct fault cores.

Type 2: Wide Fault Zones with Internally Distributed Strain

In contrast to the Pescadores fault, the central Borrego fault section has a gentler dip (40° to 50°), accommodates twice as much cumulative slip (6–8 km), and has a fault zone that is more than five times wider, averaging ~100 m and locally reaching ~175 m (Figs. 4B and 7). The wide damage zone is composed of highly fractured rock and contains numerous cores defined by high-strain fault rocks including noncohesive gouge, foliated gouge, and cohesive crush breccia (Fig. 8). In general, the fault cores vary in width from 10 to 100 cm. The rocks that make up the fault zone along this section of the Borrego fault are overwhelmingly derived from the footwall, which is composed of an intrusive complex that ranges from foliated diorite to non-foliated granite. These rocks are easily distinguished from the hanging wall, which is composed of synrift clastic sedimentary strata (Fig. 2; Barnard, 1968; Chora-Salvador, 2003). The low involvement of hanging wall strata within the fault core may reflect the relatively short duration that the hanging wall sediments have been in fault contact. Therefore, at depths below this structural basin where the hanging wall is composed of pretectonic crystalline basement, the fault zone width may be greater than that documented at the surface.

Scarps of the EMC rupture are generally distributed throughout the core and damage zone of the central Borrego fault (Figs. 7A and 8B), and coseismic slip averages ~2.8 m with a 1:1 ratio of lateral:vertical slip (Fletcher et al., 2014). Some scarp-forming faults follow a moderately dipping core near the base of the damage zone (Fig. 7B), and, in general, the structurally highest fault strands occur below the upper tectonic contact between fault zone and sedimentary basin fill (Fig. 4B). The fabric of the rupture zone is defined by a parallel-anastomosing pattern, and some sections contain up to 20 individual scarps (Fig. 4B). In contrast to the Pescadores fault segment, en echelon arrays are exceedingly rare. The orientation of almost every individual scarp-forming fault is subparallel to the upper and lower boundaries of the fault zone, and the rake of coseismic slip on most individual scarps is similar to that of total coseismic slip integrated from all scarps in a given transect. Thus, the sense of coseismic slip is not strongly partitioned among the numerous scarps within the central section of the Borrego fault. Nonetheless, faults with an antithetic

TABLE 1. FAULT SECTIONS OF THE SIERRA CUCAPAH, NORTHERN BAJA CALIFORNIA, MEXICO

Fault section	Protolith	Fault zone width (km)	Cores	Offset (km)	Alpha* (degree)	Fault zone type†
Pescadores	quartz-feldspathic	20–50	single	4.4	20–30	type 1
Northern Borrego	quartz-feldspathic	20–50	single	6–8	10–30	type 1
Laguna Salada	quartz-feldspathic	<100	single	>11	20–40	type 1
Paso Superior ramp	quartz-feldspathic and micaceous	<100	single	0.3–2.0	30–50	type 1
Central Borrego	quartz-feldspathic	100–200	multiple	6–8	40–50	type 2
Paso Superior flat	micaceous	100–200	multiple	>10	50–70	type 3

*Angle between fault and maximum compressive stress.
†See text for descriptions.

west-down sense of vertical displacement were present along a short section, which indicates that some slip transfer occurred between the master fault and the scarp-forming faults. (Fig. 2).

Along the central section of the Borrego fault, coseismic slip of the 2010 EMC event is distributed among multiple overlapping scarps, which in some transects include as many as 18 individual scarps (Fig. 4B). Thus, principal scarps were difficult to identify and no scarp was observed to accommodate more than 90% of the total coseismic slip. Moreover, principal scarps with 60%–90% of the total coseismic slip were only observed along four nonadjacent sections, none of which extend more than 600 m along strike (Fig. 4B). More commonly, surface rupture along the Borrego fault displays at least two overlapping fault scarps carrying 30%–60% of the slip together with numerous other scarps carrying 0%–30% of the slip (Fig. 4B).

The Borrego fault preserves evidence that the localization of slip on a primary fault trace may vary from one event to the next. Paleoscarps that formed in the penultimate event are sporadically preserved (Fig. 9; Hernandez Flores et al., 2013; Hernandez Flores, 2015) where cutting the oldest regionally correlative alluvial fan surface, which is likely late Pleistocene in age based on its well-developed argillic and carbonate-bearing soil horizons (Mueller and Rockwell, 1995;

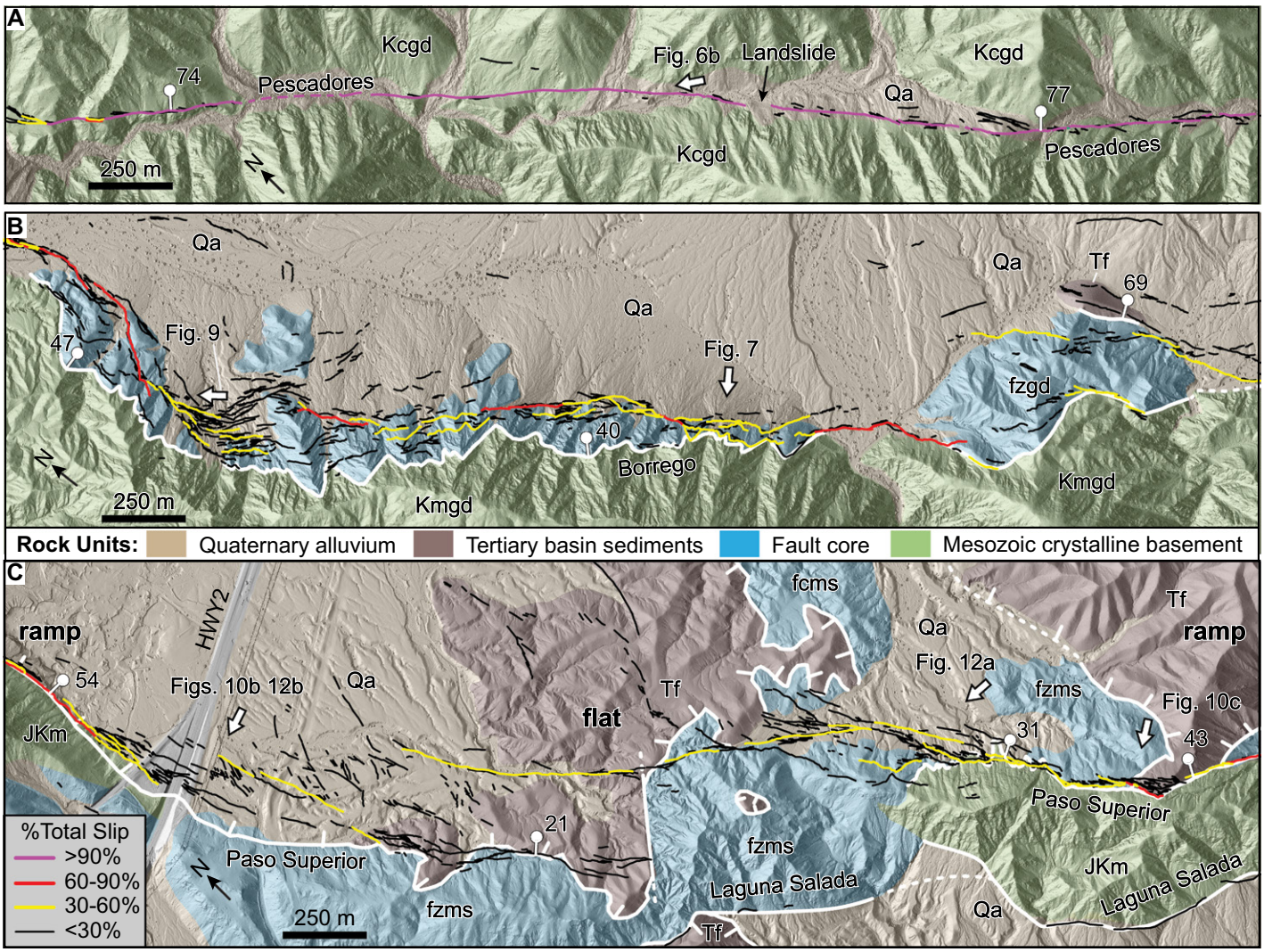

Figure 4. Simplified geologic maps showing the distribution of 2010 El Mayor–Cucapah, coseismic slip along sections of the (A) steeply dipping Pescadores fault, (B) moderately dipping Borrego fault, and (C) a flat section of the Paso Superior detachment that is flanked by two moderately dipping ramps—see Figure 2 for map locations. Teran et al. (2015) classified individual scarp traces by their relative magnitude of the total coseismic slip as observed in the field by Fletcher et al. (2014) and differential light detection and ranging data prepared by Oskin et al. (2012). Upper and lower limits of fault zone (blue map units) defined by white lines and detachment faults indicated with tic mark ornamentation. The Pescadores fault has a simple narrow fault zone that generally does not exceed 20 m in width, and thus along strike variations in width cannot be shown at this map scale. Fault zone limits are defined by the transition to more resistant outcrops of less damaged protolith (Teran et al., 2015). Dip and dip direction are shown by bar and ball symbols. Rock units include: Qa—Quaternary alluvium; Tf—Tertiary fluvial sediments; Kgd—Cretaceous granodiorite; Kmgd—Cretaceous melanocratic granitoid; JKm—Mesozoic metasedimentary rocks; fzms—fault zone composed of metasedimentary rocks; fzgd—fault zone of granodioritic composition. White arrows show azimuth of photos shown in other figures. Geology simplified from Barnard (1968), Chora-Salvador (2003), and this study using observations from the field and Google Earth. Hillshade digital elevation models downloaded from www.opentopography.org.

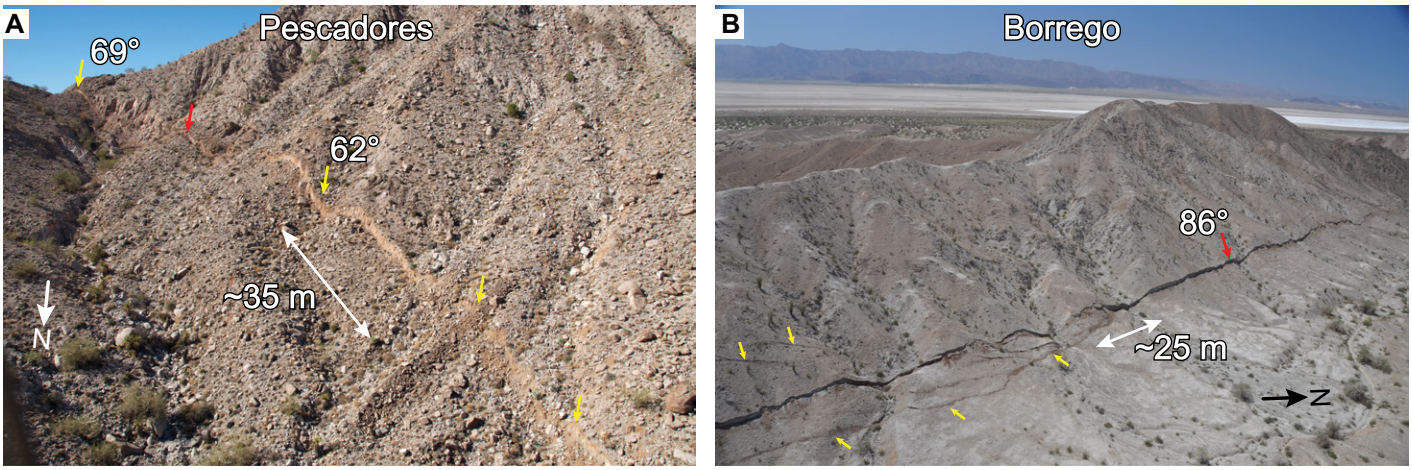

Figure 5. Oblique aerial photographs showing the rupture zone fabric developed in the 2010 El Mayor–Cucapah (EMC) event as observed along faults with a simple narrow architecture. (A) Pescadores fault dips steeply to the northeast, and >90% of total coseismic slip was typically accommodated by a single principal displacement scarp (yellow arrows). Total coseismic slip of 2.14 m (dextral slip of 1.89 m and vertical slip of 0.93 m) was measured at the red arrow. Photo azimuth is ~186° and location shown on Figure 2. (B) The subvertical sections of the Borrego fault were also characterized by a single principal displacement scarp that accommodated >60% of the total 2010 EMC coseismic slip. Yellow arrows point to synthetic thrust-fault scarps in the hanging wall and oblique Riedel shears in the footwall of the principal scarp. Total coseismic slip of 3.17 m (dextral slip of 2.88 m and vertical slip of 1.3 m) was measured at the red arrow. Photo azimuth is ~275° and location shown on Figure 2. Coseismic slip reported by Fletcher et al. (2014).

Spelz et al., 2008). Due to the highly restricted distribution of this fan surface and the long recurrence interval since the penultimate event, these paleoscarps are poorly preserved. Nonetheless, all preserved paleoscarps were reactivated in the 2010 EMC event and one locality confirms the existence of multiple overlapping scarps in the penultimate event (Fig. 9). These structural relationships suggest a certain repeatability of the pattern of surface rupture in consecutive events. However, in one case, a paleoscarp with ~4 m of vertical offset was reactivated with only 25–45 cm of vertical slip in the 2010 EMC event. Detailed mapping and trenching shows that this large-offset paleoscarp formed in a single event (Hernandez Flores et al., 2013; Hernandez Flores, 2015), and thus it carried at least 60%–90% of the coseismic displacement in the previous event. In contrast, the 2010 EMC event did not produce an obvious principal displacement scarp along the same fault section.

Type 3: Wide Fault Zones with External Subsidiary Faulting and Strain Partitioning

The Paso Superior detachment illustrates the key characteristics of a wide, complex fault zone architecture. The fault zone reaches 170 m in thickness with discrete high-strain cataclasite and gouge zones distributed throughout. Gouge zones that reach ~2 m in thickness are commonly found along the contact that separates footwall derived fault rocks from syn-rift strata of the hanging wall basin (Fig. 10). Foliated clay gouge near the contact may show a change in color from greenish/blackish hues to brownish/reddish hues reflecting incorporation of both the footwall and hanging wall protoliths, respectively. We also observe footwall-derived clay gouge in direct contact with weakly fractured sedimentary strata, and essentially no gouge derived from the hanging wall. As observed with other faults, the base of the gently dipping fault zone is well defined by an abrupt change in fracture intensity. The damage zone contains numerous different fault rocks including: thin (<2 cm) discrete slip surfaces, chloritically altered fault breccia, and strongly cohesive cataclasite (Fig. 11). The intensity of cataclasis through the damage zone is heterogeneous and we commonly observe numerous anastomosing high-strain zones separated by lenses of variably fractured protolith. Rocks in the damage zone are derived from the footwall, which consists of a lithologically heterogeneous metamorphic and igneous protoliths. Among other rock types, the damage zone contains rheologically weak protoliths such as phyllosilicate rich schists, gneiss, and marble. Strain is commonly concentrated into the weaker phyllosilicate-rich rock types as well as along contacts between rock types with strong mechanical contrasts. The damage zone of the Paso Superior detachment commonly displays a strong lithologic layering that may either represent tectonic transposition of the heterogeneous protolith or guiding of fractures along the anisotropic metamorphic layering (Fig. 12A).

Along most of the Paso Superior detachment, the EMC rupture had oblique slip with an average of 1.5 m dextral and 1.1 m of normal displacements (Fletcher et al., 2014). However, the fabric of the EMC rupture shows systematic variations that coincide well with ramps and flats of the master fault (Figs. 4C, 10B, and 10C). Ramp sections are formed by subsidiary faults that emanate from the structurally lower portions of the fault zone and displace cores and fabrics in the structurally higher portions. In the steepest portions of the ramp sections, the EMC rupture is narrowest (thickness generally <50 m) and scarps show predominantly parallel-anastomosing arrays with minor en echelon left-stepping sets (Fig. 10C). In general, principal fault scarps are easiest to identify along the ramp sections, where they typically accommodate 60%–90% of the coseismic slip (Figs. 4C and 10B). In contrast, the EMC rupture is widest in the flat sections having a map-view width of up to 292 m and thickness of ~170 m (Figs. 4C and 10C). The along-strike transition from ramp to flat also coincides with a widening of the rupture zone and principal scarps accommodating significantly less of the total coseismic slip (Figs. 4C, 10B, and 10C). The widening of the zone is accommodated by the branching of coseismic rupture along subsidiary faults that cut the hanging wall sedimentary basin above the more shallowly dipping sections of the Paso Superior detachment (Figs. 4C and 10C). Although the Paso Superior fault has an overall width similar to that of the Borrego fault and both contain

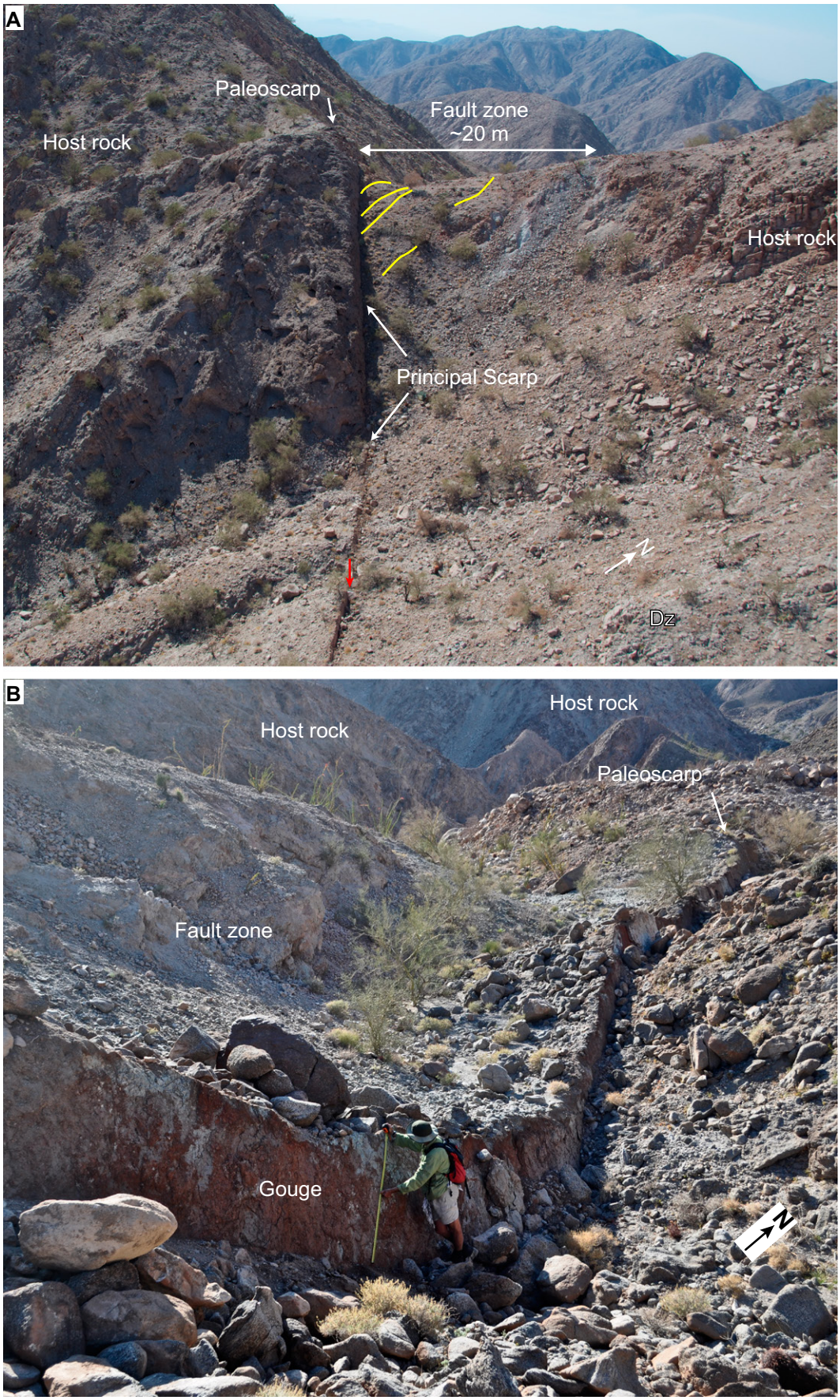

Figure 6. Field photographs of the simple narrow fault zone architecture of the Pescadores fault, southern Sierra Cucapah, Baja California, Mexico. Location shown in Figures 2 and 4A. (A) The narrow core and damage zone reach ~20 m in width and are bounded by the more resistant outcrops of the granodioritic protolith. Dextral coseismic slip of ~310 cm (red arrow; Fletcher et al., 2014) was accommodated by a single scarp that coincides with the exact location of the prominent paleoscarp observed along the ridge. Yellow lines are secondary faults that splay from the principal scarp and into the damage zone. Photo azimuth ~298°. (B) Field photo of varicolored clay gouge of the fault core, which is exposed in the free face of the principal displacement scarp. The principal scarp also coincides with a paleoscarp defined by uplifted old alluvial deposits. Tape measure indicates ~127 cm of oblique dextral-normal displacement (Fletcher et al., 2014). Photo azimuth ~294°.

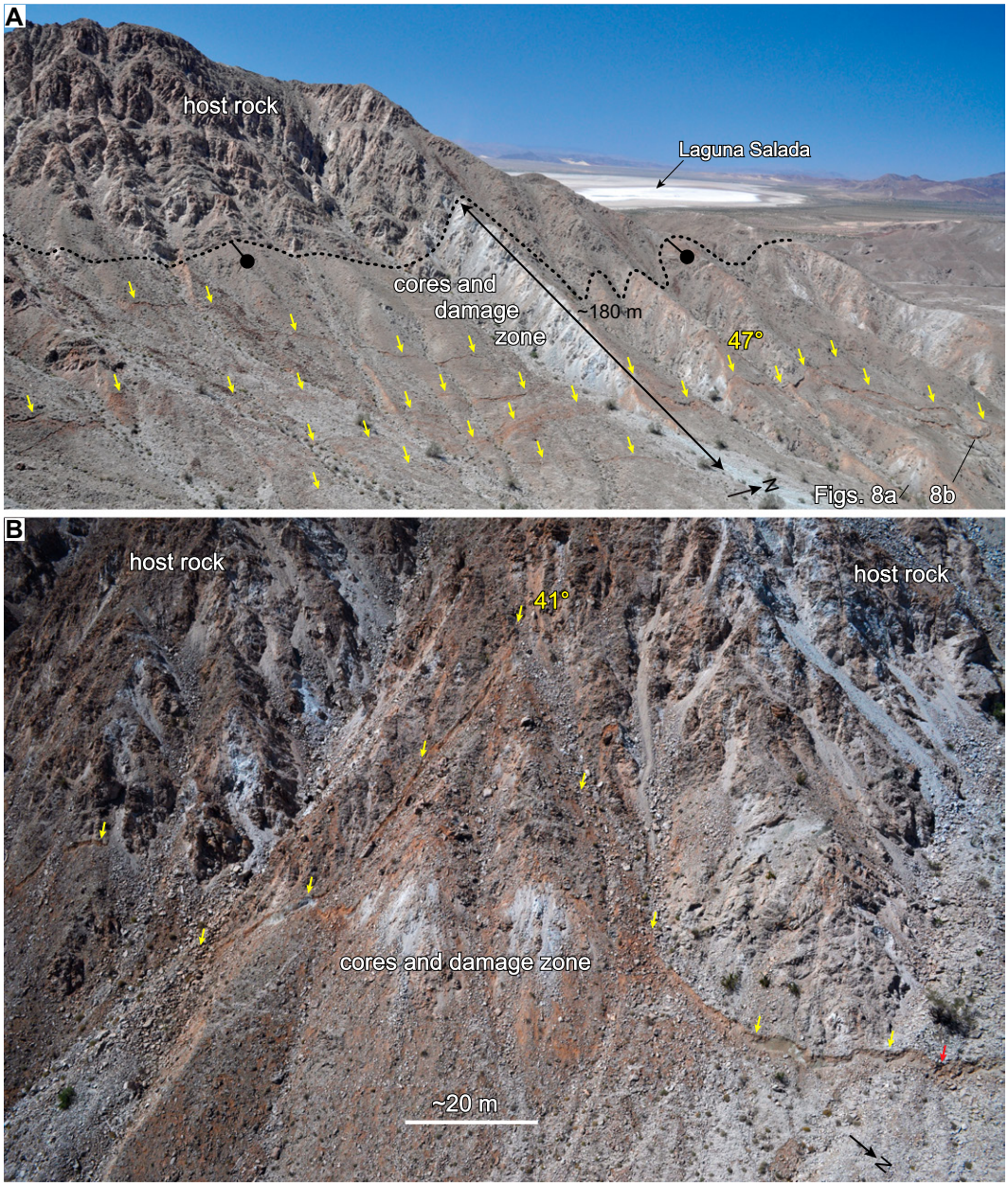

Figure 7. Oblique aerial photographs showing the rupture zone fabric of the 2010 El Mayor–Cucapah (EMC) event as observed along faults with an architecture that we classify as type 2, central Sierra Cucapah, Baja California, Mexico. Location shown in Figures 2 and 4B. (A) The moderately dipping (<50°) sections of the central Borrego fault, principal displacement scarps are generally not observed and instead 2010 EMC slip is widely distributed among numerous subparallel/anastomosing fault scarps (yellow arrows) throughout its core and inner damage zone (Dz; >130 m wide). Total coseismic slip of up to 3 m with a lateral:vertical slip ratio of ~1:1 was accommodated across the array in this fault section. Photo azimuth ~295°. (B) Oblique aerial photograph of the 2010 EMC rupture within the characteristically wide Borrego fault zone. Along the moderately dipping sections of the Borrego fault coseismic slip largely occurred within its wide damage zone, and in this photo the westernmost fault-scarp (yellow arrows) follows the footwall contact between Dz and granodioritic host rocks; it dips ~41° and accommodated 187 ± 30 and 50 ± 30 cm of vertical and dextral slip, respectively (red arrow; Fletcher et al., 2014). Bi-directional arrow for scale. Photo azimuth ~230°.

multiple high-strain cores, the former is distinguished by abundant subsidiary faults that both cut through and extend beyond the limits of the long-term fault zone. This represents a significant difference in the internal structural complexity of these two faults.

Where late Pleistocene fan surfaces that contain penultimate event scarps are preserved, we observe multiple overlapping paleoscarps with complex geometries and distributions. Although much of the detail of the penultimate surface rupture has been lost due to erosion, the complex branching of the EMC rupture coincides well with the remaining paleoscarps and, without exception, all observed paleoscarps were reactivated in this event.

Coseismic Slip Partitioning in Type 3 Faults

Flat sections of the Paso Superior detachments display the widest and most complex rupture zone fabrics from the 2010 EMC event. Coseismic slip is not only distributed among multiple scarps, but it is also partitioned kinematically into sets of scarp-forming faults with distinct orientations and slip directions. Figure 12A shows an example of spatially separated bands of scarps with distinct orientations and kinematics. Both sets have a subparallel strike and are exposed within the wide complex fault zone of the Paso Superior detachment. The set of scarps that crop out closest to the surface trace of the detachment exhibits shallow to moderate angles of inclination (50°–37°), which are only slightly steeper than the basal contact of the fault zone (31°–37°), and they accommodate predominately normal-sense coseismic slip (Fletcher et al., 2014). The set of scarps located farthest from the surface trace are subvertical and accommodate coseismic slip dominated by dextral strike slip (Fig. 12A; Fletcher et al., 2014). Farther north where the Paso Superior detachment crosses Highway 2, Figure 10B shows that scarps can be divided into at least two sets of distinctly different orientations; one set strikes subparallel to the hanging wall contact of the Paso Superior fault zone and a second includes a broad zone of left-stepping en echelon scarps that are highly oblique to the strike of the fault zone (Fig. 10A). The oblique strike and en echelon configuration

Figure 8. Field photographs of the penetratively fractured crush breccia distributed throughout the core and damage zone of the Borrego fault. Photo azimuth ~006° Taken by Geoff Faneros on 6 April, 2010. (B) Slip surface reactivated with ~1.4 m of vertical slip in the El Mayor–Cucapah event (lateral displacement not measured) exposes brecciated protolith in its free face. See Figure 7 for photo locations.

Figure 9. Field photograph of the 2010 El Mayor–Cucapah (EMC) rupture (yellow arrows) distributed throughout the wide damage zone of the Borrego fault, southern Sierra Cucapah, Baja California, Mexico. Location shown in Figures 2 and 4B. Photo also shows the 2010 EMC reactivation of multiple overlapping paleoscarps (blue arrows), which offset an old alluvial surface (red arrows). The prominent paleoscarp has ~4 m of vertical offset and likely represents the principal displacement scarp from the penultimate event (Hernandez Flores et al., 2013). However, in the 2010 EMC event a principal displacement scarp was not observed, and thus the distribution of slip magnitude is not exactly the same in consecutive earthquake rupture events. Photo azimuth of ~323°.

of the second set demonstrates that they accommodate much of the dextral wrenching across the fault zone. Another example of kinematic partitioning is documented in Figure 12B. All scarps in this photo strike subparallel to the hanging wall contact, which dips 20° at this locality, but the scarps themselves are steep to subvertical. Based on the offset of the highway pavement and lane markers, it is clear that the set of scarps that crop out closest to the surface trace of the detachment accommodates pure normal-sense dip slip, whereas the set of scarps located farthest from the surface trace accommodates pure dextral strike slip.

All of the above examples of kinematic partitioning show that despite the extreme structural complexities manifested in rupture zone fabric, there is an underlying order that implies the existence of a mechanical explanation. Wesnousky and Jones (1994) demonstrated that crustal-scale kinematic partitioning of transtensional shearing does not require changes in the state of stress to drive slip on both normal faults and strike slip faults, and they argued that kinematic partitioning on two faults is mechanically favored over oblique slip on a single fault. The 2010 EMC rupture clearly shows that whether it is favorable or not, oblique coseismic slip becomes partitioned onto multiple subsidiary faults that extend far beyond the limits of the long-lived fault zone.

In order to test the hypothesis that kinematic partitioning is consistent with a single stress state, we plotted the hypothetical and observed slip directions for all cases of partitioned coseismic slip along the Paso Superior detachment (Fig. 13A). The assumed state of stress is consistent with stress inversions performed by Fletcher et al. (2016), who showed that for the Sierra Cucapah the maximum principal stress (σ_1) is vertical, the minimum principal stress (σ_3) is horizontal trending 085°, and the intermediate principal stress (σ_2) is horizontal trending 355°. The orientations of principal stress axes were derived from the linked Bingham statistics of 237,000 stress models that make up the 95% confidence interval. The stress magnitude ratio ($\phi = (\sigma_2 - \sigma_3)/(\sigma_1 - \sigma_3)$) is assumed to be 0.98, which is the modal peak for all the stress models in the 95% confidence interval and indicates that the maximum and intermediate principal stresses are very close in magnitude (Fletcher et al., 2016). Hypothetical slip directions shown in Figure 13 are assumed to be parallel to the resolved shear stress, which is calculated by projecting the assumed stress state onto planes of different orientations (Wallace, 1951; Bott, 1959).

Figure 13A shows a strong correlation between the observed and hypothetical slip directions suggesting a cause and effect relationship, and thus it would seem that the stress state that controls the direction of fault slip at seismogenic depths also factors into controlling the complex expression of rupture zone fabric developed within a few hundred meters of the surface. One important relationship displayed in Figure 13A is that all subvertical faults regardless of strike are predicted to be dominated by strike slip. This also implies that regardless of topographic and other perturbations that may reorient principal stress axes, subvertical faults are mechanically favored to accommodate the lateral component of oblique slip. The geometry of any low-angle

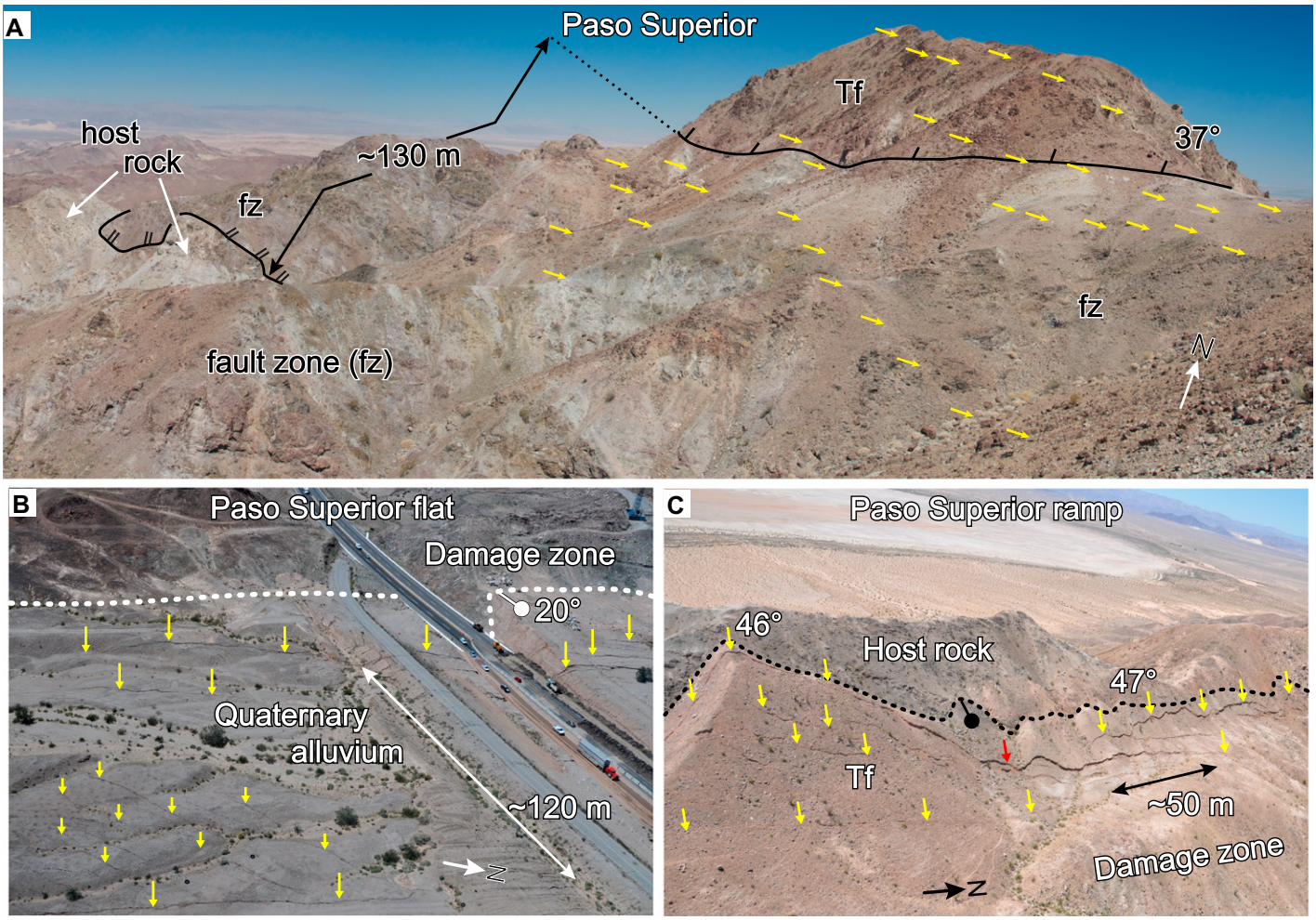

Figure 10. (A) Field photograph that shows the wide, complex type 3 fault zone (~130 m) developed along the Paso Superior detachment. Scarps of the 2010 El Mayor–Cucapah (EMC) rupture (yellow arrows) are distributed throughout the fault zone, cut the upper fault contact, and extend into hanging wall Tertiary fanglomerates (Tf). This section of the Paso Superior detachment dips ~37°, and its damage zone is composed of gouge cataclasite and breccia derived entirely from the footwall, which is dominated by protolith of layered metasedimentary rocks. Upper and lower limits of fault zone mapped as black lines with single bar and double bar ornamentations, respectively. In the 2010 EMC event, this section accommodated up to 1.3 m of total coseismic slip with a lateral:vertical ratio of ~1:2 (Fletcher et al., 2014). Photo azimuth is 330°. Location shown in Figure 2. (B) Wide complex rupture zone fabric developed along the Paso Superior detachment in a flat section of the fault that dips 11° to 20°. Coseismic slip is broadly distributed among multiple fault-scarps oriented subparallel and oblique to the master fault trace. Total coseismic slip (lateral:vertical slip ratio of ~3:1) of up to 2 m was measured across the array (Fletcher et al., 2014). Location shown in Figure 4. (C) A narrowing of the zone of coseismic rupture associated in the 2010 EMC event occurs along the southern ramp section of the Paso Superior detachment where its dip increases to 47°. Here coseismic slip is concentrated in a zone <50 m wide and scarps are arranged in predominantly parallel-anastomosing arrays with minor en echelon left-stepping sets. No single scarp accommodates more than 60% of total coseismic slip. Total coseismic slip of 1.86 m (dextral slip of 0.5 m and vertical slip of 1.22 m) measured at red arrow (Fletcher et al., 2014). Location shown in Figure 4.

fault requires that scarps farthest from the surface trace of the fault dip more steeply than those closer to the surface trace (Fig. 13B). Therefore, more steeply dipping faults should preferentially filter off the strike slip component of offset leaving the up-dip section of detachment fault and any of its fault splays with the remaining dip slip component (Fig. 13B). This explains why normal-sense dip slip is consistently partitioned into the coseismic scarps closest to the surface trace of the Paso Superior detachment and dextral strike slip is accommodated by scarps farther from the trace (Figs. 12A and 12B).

Summary of Field Relations

We demonstrate that as fault zones increase in complexity and width, so does the expression of coseismic surface rupture (Figs. 3A and 4), which supports the strong link between fault zone architecture and coseismic rupture zone fabrics as observed by Teran et al. (2015). Additionally, we have documented a suite of associated structures and fabrics that occur together in different types of fault zones, which are schematically shown in Figure 14. Fault zones of the type 1 class generally do not exceed 70 m in width and have a single well-developed core that is typically defined by a zone of foliated clay gouge of ~1 m in thickness. In this fault class, coseismic slip is strongly concentrated onto a single well-defined principal scarp that reactivates the clay gouge core (Figs. 5A and 6). Typically, these

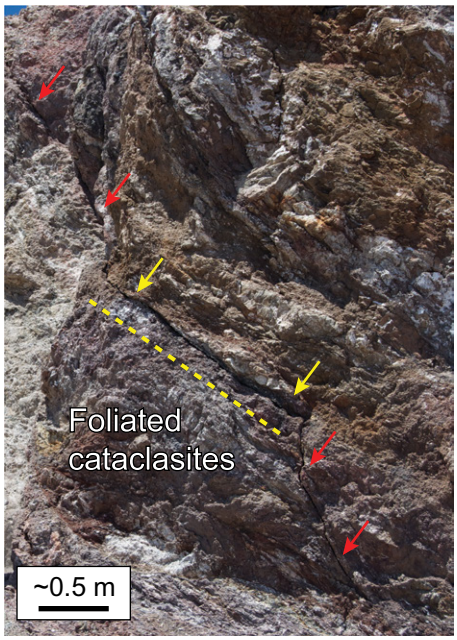

Figure 11. Field photograph of strongly foliated cataclasites in the damage zone along the northern flat section of the Paso Superior detachment. A coseismic fracture formed in the 2010 El Mayor–Cucapah event has rather small displacement but clearly demonstrates that it propagated through (red arrows), and reactivated (yellow arrows) the preexisting cataclastic foliation of the detachment fault core. Yellow dashed line is parallel to cataclastic foliation. Location shown in Figure 2.

principal displacement scarps accommodate >90% of the total coseismic slip (Fig. 4A). Fault zone complexity increases considerably in the type 2 class, which is characterized by a broader zone (50–150 m) of overlapping cores, but none of these are as well developed as the main core associated with the simple narrow class. This widening of the fault zone is accompanied by widening of the coseismic rupture zone and an increase in the number of scarps. In type 2 fault sections, it is difficult to identify a single principal scarp, and scarps with the greatest coseismic displacement are generally limited in both along-strike length (<600 m) and the relative amount of coseismic slip that they accommodate (30%–60%; Fig. 4B). In this way, the rupture fabric strongly reflects the fault zone architecture characterized by multiple overlapping cores and subsidiary faults. Rupture zones of the type 3 class are similar to those of the type 2 class, but they are distinguished by abundant subsidiary faults and strong coseismic slip partitioning. These widest and most complex rupture zones are associated with the widest and most complex fault zones. However, coseismic surface rupture is generally not restricted to the confines of the long-lived fault zone. Instead most scarp-forming faults splay from the main fault to form new ramps that uplift the footwall or occur as extensive and structurally complex arrays in the immediate hanging wall (Fig. 14C). Scarps that have <30% of the total coseismic slip were observed in all fault classes.

Gouge Production and Fault Zone Architecture

The diversity of fault-zone architecture and related rupture zone fabrics in the Sierra Cucapah provides an opportunity to assess their underlying controls. Yoshioka (1986) identified multiple factors that affect gouge production in laboratory experiments including displacement, rock strength, normal stress, existence of gouge prior to slip, and mode of slip. Based on measurements of the amount of gouge produced in laboratory conditions, rock strength and normal stress are by far the most important of the five factors (Yoshioka, 1986). In examples of natural faults, cumulative displacement has been shown to affect some components of fault zone architecture such as the abundance of gouge in fault cores (e.g., Scholz, 1987; Hull, 1988), as well as the intensity of fracturing and overall width of damage zones (Shipton and Cowie, 2001; Mitchell and Faulkner, 2009). Protolith strength is also thought to strongly affect the width and number of cores (e.g., Faulkner et al., 2003). Given the importance of normal stress in experimental gouge production, surprisingly little work has been done to examine its effects on the architectural expression of faults. In this study we show how fault orientation can be used as a proxy for normal stress. Additionally we compare the relative importance of displacement, protolith, and orientation-controlled normal stress on the resulting architectural variations of faults in the Sierra Cucapah.

Displacement

We find that cumulative displacement on faults with several kilometers of slip does not appreciably affect fault zone architecture compared to other factors. One of the faults with the greatest cumulative slip in the study area is the Laguna Salada fault. In terms of the range of architectural styles documented in this study, the Laguna Salada fault is most similar to the type 1 class represented by the Pescadores fault (Table 1; Figs. 4A, 5A, and 6). Both faults have a single high-strain core and cut quartzo-feldspathic protoliths. They also have similar orientations and oblique dextral-normal slip directions. However, the Laguna Salada fault has accommodated more than twice as much cumulative slip (>11 km versus 4.4 km). The Paso Superior detachment is the only other fault in the Sierra Cucapah with cumulative slip that approaches that of the Laguna Salada fault, yet its damage zone, hosting multiple fault cores, belongs to the type 3 class of faults at the opposite end of the spectrum of structural complexity. Therefore, structural relations in the Sierra Cucapah show that faults with much different cumulative slip have similar architecture and those with similar slip have radically different architecture, which suggests that the magnitude of slip has the smallest effect on fault zone architecture.

Protolith

Protolith appears to exhibit a stronger control on gouge production than displacement. The two extremes of architectural variations in the Sierra Cucapah are represented by faults that have very different protoliths. The wide complex fault zone of the Paso Superior detachment is developed in a sequence of phyllosilicate-rich metasedimentary gneiss with a strong preexisting foliation. In contrast, many simple narrow fault zones in the Sierra Cucapah are developed from quartzo-feldspathic protoliths of the granitoid plutonic complex. Laboratory experiments demonstrate an inverse relationship between production of gouge and the strength of the host rock (Yoshioka, 1986) and quartzo-feldspathic protoliths are much stronger than phyllosilicate protoliths, which commonly have a preexisting mechanical fissility that is susceptible to reactivation (Faulkner et al., 2003). There is a general perception that cataclasis of a quartzo-feldspathic protolith is associated with strain weakening, which has a positive feedback with strain localization and results in the development of a narrow fault zone with a single high-strain core (Chester and Logan, 1986; Chester et al., 1993; Faulkner et al., 2003, 2008). In contrast, phyllosilicate host rocks are associated with multicore fault zones, which are thought to develop because of strain hardening during cataclasis (Faulkner et al., 2003, 2008).

The frictional strength of faults is typically assumed to obey Byerlee's (1978) law with a coefficient of friction of 0.6–0.85. However, most of these friction measurements were performed on joints and other bare rock surfaces and more recent work has shown that clay rich gouges are consistently weak, with a steady-state coefficient of sliding friction of <0.35 (Saffer and Marone 2003; Ikari et al., 2009). Collettini et al. (2009) showed that even in rocks with relatively low abundance of phyllosilicates (10%–30%), the frictional properties of the rock may approach

Figure 12. Photographs of the strong kinematic partitioning of 2010 El Mayor–Cucapah (EMC) rupture zones along the shallow dipping sections of the Paso Superior detachment, northern Sierra Cucapah, Baja California, Mexico. Location shown in Figures 2 and 4B. (A) Oblique aerial photograph showing two main sets of fault scarps. Moderately dipping scarps with dominantly dip-slip motion are shown with yellow arrows, and subvertical scarps with dominantly strike-slip are shown with red arrows. The colored circle and triangle symbols mark pairs of sites of partitioned slip measurements used in Figure 13. In the distance both sets of coseismic scarps cut across the upper fault contact and project into the adjacent hanging wall. The well exposed fault core is composed of a thick (~90 m) package of smeared metasedimentary rocks (fcms) with compositional layering shown by a dash-dot line pattern. Hanging wall Tertiary fanglomerates (Tf; upper right of photo) and footwall Jurassic–Cretaceous gneissic rocks (JKm; upper left of photo). Upper and lower limits of shear zone marked by black lines with single bar and double bar ornamentation, respectively. Numbers indicate dip of scarps and faults. Photo azimuth ~280°. (B) Field photograph at Highway 2 where 2010 EMC rupture developed almost entirely as off-fault deformation in the hanging wall sediments (Qa) located immediately above the 20° dipping Paso Superior detachment. Offset road markings clearly show that scarps in the upper half of the photo accommodated dominantly normal-sense vertical offsets, whereas scarps in the lower half of the photo show dominantly dextral displacements. Photo azimuth is ~215°.

that of the weak phyllosilicate phases. Most of the phyllosilicate phases observed in fault zones are secondary and derived from grain-size reduction and synkinematic hydration reactions associated with shearing. However, metamorphic rocks containing abundant primary phyllosilicates are also common in continental crust. Significant weakening associated with the reactivation of metamorphic anisotropies is well documented (e.g., Donath, 1961). As proposed by Faulkner et al. (2003, 2008), phyllosilicate-rich protoliths and the fault rocks derived from them should have a very low contrast in frictional strength. As we argue below, the process of cataclasis of anisotropic phyllosilicate rich protolith is inherently characterized by strain hardening, which leads to the development of wide multicored fault zones.

Fault Orientation

Fault orientation controls the expected ratio of normal stress to shear stress, which in this transtentional setting should be higher for faults with

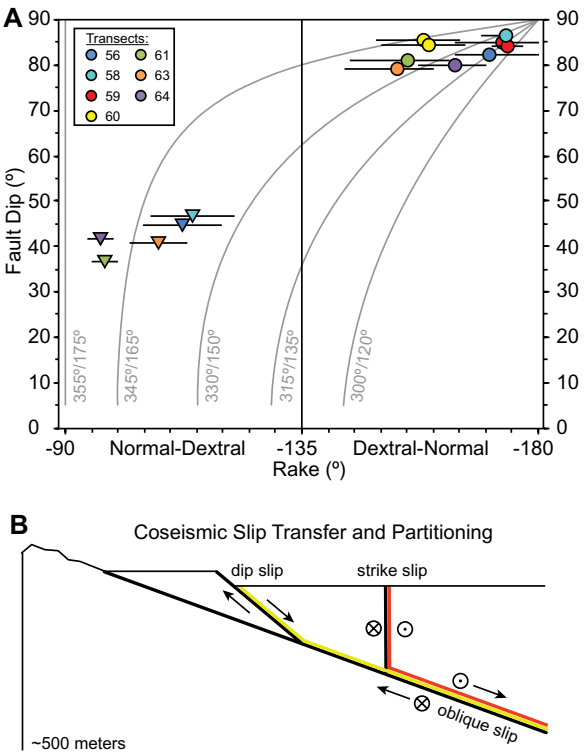

Figure 13. Structural analysis of coseismic slip partitioning on the Paso Superior detachment, northern Sierra Cucapah, Baja California, Mexico. Location shown in Figures 2 and 4B. (A) Plot showing strong correlation of observed (circles and triangles colored by transects, some of which are shown in Fig. 12) and theoretical slip directions (pale gray lines) expressed as rake for faults of different orientations. Theoretical slip direction is calculated by projecting regional stress modeled by Fletcher et al. (2016) onto planes of different orientations. Grey lines show theoretical rake of slip for planes of constant strike and variable dip. For faults of a wide range of strikes, the theoretical strike slip component of oblique offset becomes progressively greater as dip increases, such that subvertical faults of any strike are predicted to have little to no dip slip. Observed coseismic slip on shallowly dipping scarps from up-dip portion of the transects (triangles) is dominated by dip slip, and that from steeply dipping scarps from the down-dip portion of the transects (circles) is dominated by strike slip. (B) Schematic cross section showing observed patterns of coseismic slip partitioning on the Paso Superior detachment. Portions of the fault activated by strike slip are shown in red, and those activated by dip slip are shown in yellow. Scarp-forming faults farthest from the surface trace of the detachment are steeper and preferentially accommodate the strike slip component of coseismic displacement. The remaining coseismic dip slip propagates onto more gently inclined scarp forming faults located closer to the surface trace of the detachment.

lower dip (e.g., Fletcher et al., 2016). Indeed, one of the most surprising results from both this study and the companion paper by Teran et al. (2015) is that fault zone architecture changes systematically with orientation, becoming increasingly wider and more complex with decreasing dip of the structure (Fig. 3). For the examples we describe here, however, both elevated relative normal stress and a weaker protolith may be responsible for the wide Paso Superior fault zone. Thus to discriminate these effects, we turn to the central Borrego fault example. The central Borrego fault has cumulative slip (6–8 km) that is intermediate between that of the Pescadores fault (~4 km) and Laguna Salada fault (>11 km). All of these fault sections cut strong quartz-feldspathic protoliths, but the former shares almost no similarities in structural style with the latter two (Table 1). The central Borrego fault zone is characterized by penetrative fracturing and crush breccia that is distributed throughout its wide type 2 fault zone. None of the high-strain zones within the Borrego fault zone reach the same thickness and degree of comminution as the single fault core observed on the type 1 Pescadores fault zone. Therefore, although strain is not as intense in the central Borrego fault, it is more broadly distributed through a fault zone that is 3–5 times wider. Besides the vastly different fault zone architectures, the only significant difference between these faults is their orientations. The narrow type 1 faults are both steeply dipping, whereas, the wide type 2 fault is moderately dipping (Table 1).

Further evidence for the effect of orientation on fault zone architecture is provided by along strike variations with dip of some of the faults in the Sierra Cucapah. North of the moderately dipping central section, the Borrego fault becomes subvertical, and this change in orientation is accompanied by the transition into a narrow type 1 fault zone (Table 1; Fig. 5B). Here strain becomes concentrated onto a single core composed of foliated gouge and the 2010 EMC rupture zone fabric is dominated by a single principal displacement scarp (Fig. 5B; Dorsey et al., 2017; Teran et al., 2015). In yet another example, the widest and most complex rupture zone fabrics developed in the 2010 EMC event are observed along the ~20° dipping flat sections of the Paso Superior detachment. In contrast, the along-strike ramp sections of the Paso Superior fault (40°–60° dip) exhibit a 105-fold decrease in rupture-zone thickness (Figs. 3, 4C, 10B, and 10C). Because the ramp sections offset structurally higher portions of the fault zone, these faults have developed with far less slip than the master Paso Superior detachment into which they root (Fig. 14C). Thus the along-strike occurrence of ramps and flats along the Paso Superior detachment coincides well with the transition from type 1 to type 3 fault zones, respectively.

We propose that the correlation of fault zone architecture with orientation can be explained by considering how orientation determines the traction that a fault experiences. All fault sections in this study that were activated in the 2010 EMC earthquake and coseismic slip directions, despite their great diversity, are consistent with a uniform regional stress state, which was derived by Fletcher et al. (2016) as previously described for Figure 13. A Mohr plot of this stress state demonstrates that the observed variation in normal stress on individual fault sections approaches the applied differential stress (Fig. 14), which is of the order of tens of megapascals at depths of earthquake nucleation (e.g., Fletcher et al., 2016). In this transtensional tectonic regime, the degree of misorientation and resolved normal stress both increase as fault dip decreases (Fig. 14D). The three classes of faults that we have documented in this study plot in the Mohr diagram over distinct ranges of slip tendencies, and generally faults of types 1, 2, and 3 have high, intermediate, and low slip tendencies, respectively (Fig. 14).

Laboratory experiments (e.g., Yoshioka, 1986) and numerical modeling (e.g., Moore and Lockner, 2007) demonstrate a strong positive correlation between gouge production and normal stress. This is consistent with qualitative observations from the Sierra Cucapah where gently dipping and wide fault zones with multiple cores generally contain more gouge than narrow single-core faults. However, the expected variation in gouge production alone does not explain the complex branching and development of multiple high-strain cores in a single fault zone.

Faults oriented at a high angle to the maximum compressive stress experience high normal stress and are considered misoriented because they have the greatest resistance to activation (Fig. 14D). In order to reach criticality and slip, misoriented faults require low-frictional strength

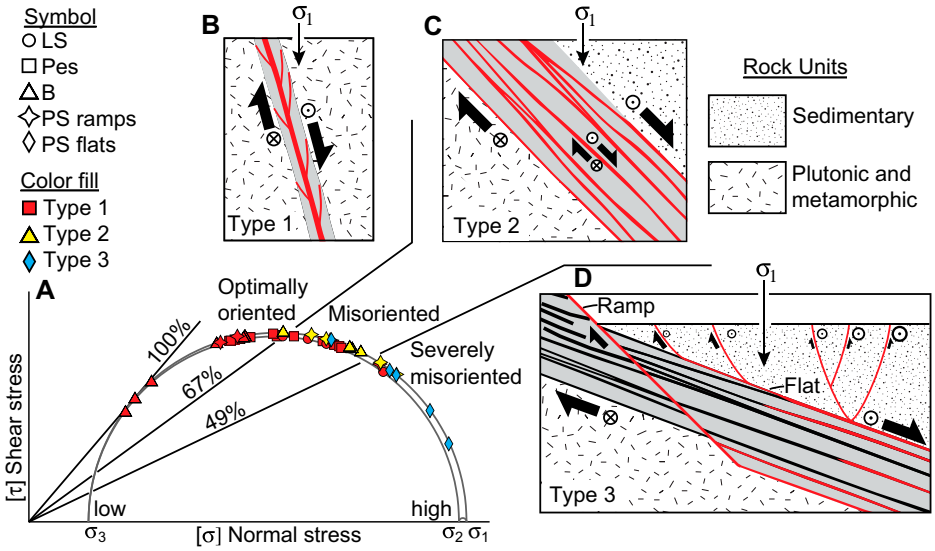

Figure 14. Mohr circle plot and schematic cross sections showing the three main classes of fault and rupture zones in the Sierra Cucapah, northern Baja California, Mexico. (A) Mohr circle plot of all fault sections activated by the 2010 El Mayor–Cucapah (EMC) rupture. The position of each data point is calculated by projecting regional stress on to the average orientation of the fault zone in each section. Regional stress was calculated by Fletcher et al. (2016). Each fault section was classified according to structural style of their fault and rupture zones, which are shown in the following schematic cross sections: (B) simple narrow, (C) intermediate, and (D) wide and complex. Schematic fault cores and/or subsidiary faults are shown in red if they accommodated coseismic slip in the EMC rupture or black if they did not. Slip tendency is the shear:normal stress ratio normalized to a maximum of 100% for the most optimally oriented fault (Morris et al., 1996). Lines of constant slip tendency have different slopes in part A. Type 1 faults have high slip tendency (49%–100%) and low normal stress. Type 3 faults have low slip tendency (<60%) and high normal stress. Type 2 faults have intermediate slip tendency. Fault abbreviations include: B—Borrego; LS—Laguna Salada; PS—Paso Superior; Pes—Pescadores.

(Carpenter et al., 2011; Lockner et al., 2011), high pore pressure (e.g., Rice, 1992; Axen, 1992), and/or high differential stress (e.g., Nieto-Samaniego and Alaniz-Alvarez, 1995, 1997; Nieto-Samaniego, 1999; Axen, 2004; Fletcher et al., 2016). Fletcher et al. (2016) showed how stress can rise to the magnitudes required to make misoriented faults slip, even in the presence of nearby optimally oriented faults that yield at much lower states of differential stress. However, regardless of the specifics of any given stress condition, a fault must somehow reach criticality in order to slip. All of the factors that affect criticality should operate on the entire fault zone. Therefore, if the misoriented surfaces in a fault zone are able to reach criticality, others with more optimal orientations should also be critically loaded. We propose that the frictional reactivation of slip surfaces with a greater range of orientations is one important factor that causes the branching of slip onto multiple paths and leads to a widening of the fault zone.

In severely misoriented fault zones, it could be possible for coseismic rupture to leave the fault zone altogether and follow more optimally oriented faults in adjacent blocks, which is essentially what we observe along the Paso Superior detachment. Flat sections of the detachment are associated with broad scarp arrays developed in the hanging wall immediately adjacent to the surface trace of the fault zone. Alternatively, ramp sections are controlled by splays that emanate from near its base and cut across the fabric of the long-lived fault zone (Fig. 14C). Coseismic scarps in both ramp and flat settings either leave the long-lived, severely misoriented fault zone or cut across it. Similar structural relationships are commonly observed in other well studied examples of seismically active low-angle normal faults (e.g., Caskey et al., 1996; Axen et al., 1999; Hayman et al., 2003; Numelin et al., 2007; Spelz et al., 2008; Fletcher and Spelz, 2009). Fletcher and Spelz (2009) proposed that the near-surface transfer of slip from the low-angle master fault to more optimally oriented high-angle scarp-forming faults occurs because the factors that are thought to allow seismogenic slip on low-angle faults at depth, such as near-lithostatic pore fluid pressure (Axen, 1992) or rotation of principal stress axes (Yin, 1989; Melosh, 1990), are not as likely to operate near the surface. Also, near the surface, high-angle faults are not as likely to be pinned against other faults within the overall fault network, allowing these to be activated as slip on a low-angle fault propagates to the surface.

Implications for the San Andreas and Other Misoriented Faults

The San Andreas fault is the main plate boundary fault between the Pacific and North America plates (Fig. 1) and has accommodated hundreds of kilometers of cumulative slip (Matthews, 1976). It extends ~1300 km and transects numerous distinct tectonostratigraphic terranes such as the Franciscan accretionary wedge, underplated Pelona-Orocopia-Rand schist, the Mesozoic batholiths of the Sierra Nevada and Peninsular Ranges, as well as a diverse suite of metamorphic and plutonic rocks of the Proterozoic North American craton. Two contrasting sections of the San Andreas fault, discussed below, demonstrate the relative effects of host rock lithology, mode of slip, cumulative slip, and normal stress on the internal structure of a fault zone.

The Parkfield section of the San Andreas fault in central California, USA, consists of a complex zone of faulting that is ~3 km wide and made up of overlapping strands including the Buzzard Canyon, San Andreas, and Gold Hills faults, each of which contains multiple cores (Rymer et al., 2006; Bradbury et al., 2011). Host rock lithology is thought to play a primary role in controlling the dominantly creeping mode of slip in this section, and high-strain gouge zones contain talc and other weak phyllosilicates derived from hydrothermal alteration and shearing of serpentine-rich ultramafic rocks in contact with arkosic sandstones, both of which are abundant within the Franciscan mélange (Moore and Rymer, 2007, 2012).

The Mojave section of the San Andreas fault in southern California predominantly cuts schist and quartzo-feldspathic rocks derived from Proterozoic basement and the Mesozoic batholith (Barrows et al., 1985). Mode of slip is thought to be dominated by stick-slip and this section was activated most recently in the 1857 Mw 7.8 Fort Tejon earthquake, which had as much as 8 m of right-lateral coseismic slip (Sieh, 1978; Zielke et al., 2010). Near Littlerock, California, the San Andreas system is composed of six major strands including from NE to SW: the Littlerock fault, San Andreas main fault, northern and southern Nadeau faults, Punchbowl fault, and Soledad fault as well as several other unnamed strands

TABLE 2. GLOBAL SURVEY OF WIDE COMPLEX FAULT ZONES

Fault	Fault zone width (km)	Number of cores	Offset (km)	Slip mode	Protolith	Alpha (degree)*
San Andreas Parkfield	3†	>4†	315§	Creep#	Phyllosilicate#	70–90**
San Andreas Mojave	1–3††	>6††	315§	Stick slip§§	Quartz-feldspathic and phyllosilicate**	60–80**
Carboneras	0.75##	>2##	40***	Creep and stick slip##	Phyllosilicate##	60–90***
Caleta Coloso	0.2–0.3##	>2##	>5***	Stick slip##	Quartz-feldspathic##	80–90***
Gole Larghe	0.6†††	2†††	1.1†††	Stick slip†††	Quartz-feldspathic†††	80–90†††

*Angle between fault and maximum compressive stress.
†Rymer et al. (2006); Bradbury et al. (2011).
§Mathews (1976).
#Moore and Rymer (2007, 2012).
**Zoback et al. (1987); Yang and Hauksson (2013).
††Barrows et al. (1985).
§§Sieh (1978); Zielke et al. (2010).
##Faulkner et al. (2008).
***Stapel et al. (1996); Faulkner et al. (2008).
†††Di Toro and Pennacchioni (2005); Smith et al. (2013).

(Barrows et al., 1985; Dor et al., 2006). The faults are subparallel in strike, define an anastomosing configuration and each strand represents a distinct core in a complex multicore fault zone that varies in width from 1 to 3 km (Barrows et al., 1985; Dor et al., 2006). It is difficult to unequivocally define the slip history of each individual strand, but each of them has accommodated tens of kilometers of slip since the early Pliocene (4.5–4.0 Ma; Barrows et al., 1985; Powell, 1993). Most late Quaternary slip has been concentrated on the main strand of the San Andreas fault, which is thought to be much younger than the other strands, having initiated in the Pleistocene. Nonetheless, Sieh (1978) proposed that an observed slip deficit of the 1857 Fort Tejon rupture near Palmdale, California can be explained by having additional coseismic slip partitioned onto adjacent strands in the overlapping system.

One factor that is consistent with our example in the Sierra Cucapah and may best explain the kilometer-scale width and complexity of the San Andreas fault zone is high normal stress. The San Andreas is severely misoriented and typically forms angles of 60°–90° to the horizontal maximum compressive stress (e.g., Zoback et al., 1987; Yang and Hauksson, 2013; Fletcher et al., 2014). Explaining the mechanics of slip on the San Andreas has been one of the greatest conundrums in earth science and leading hypotheses include: (1) high pore pressure with stress rotation in the fault zone (Rice 1992; Faulkner et al., 2006), (2) heterogeneous friction with the San Andreas fault as the weakest in the system of faults (Lockner et al., 2011), and (3) uniform friction among multiple faults that form an interlocking network with the San Andreas as the strongest member due to its severe misorientation (Fletcher et al., 2016). Regardless of the controversy associated with slip mechanics, there is a strong consensus that the San Andreas fault has a very low slip tendency and thus must have very high applied normal stress.

Faulkner et al. (2008) presented a detailed structural analysis of two other large-scale strike-slip faults with wide multi-cored fault zones. Despite strong similarities of fault zone architecture, the Carboneras fault of southeastern Spain and the Caleta Coloso fault of northern Chile differ markedly in protolith (graphitic mica schist versus granodioritic plutonic rocks), cumulative slip (40 versus >5 km), and tectonic setting (transtension versus transpression), respectively (Stapel et al., 1996; Faulkner et al., 2008). However, the one parameter that is common to both of them, is low slip tendency and thus high applied normal stress. The Carboneras fault regionally forms an angle of 60° to the maximum compressive stress, and locally it becomes as high as 90° (Stapel et al., 1996; Faulkner et al., 2008). The Caleta Coloso fault is oriented 80°–90° from the modern regional maximum compressive stress (Faulkner et al., 2008; Heidbach et al., 2009).

The Gole Larghe fault zone, which splays from the Tonale line in the Italian Alps, is another example of a well-studied wide complex fault zone. Despite having accommodated only 1100 m of total dextral displacement, the Gole Larghe fault zone is ~600 m wide and composed of numerous overlapping pseudotachylyte and cataclasite bearing faults in addition to two prominent zones of 2-m-thick cataclasites (Di Toro and Pennacchioni, 2005; Smith et al., 2013). The fault zone is developed in quartzofeldspathic rich protolith that forms part of the Adamello tonalitic batholith (Di Toro and Pennacchioni, 2005; Smith et al., 2013). Pseudotachylytes from the fault zone yield $^{40}Ar/^{39}Ar$–ages of 29.8 ± 0.4 Ma and their presence indicate seismogenic stick-slip behavior (Di Toro and Pennacchioni, 2005). The Oligocene maximum compressive stress in this region is oriented subhorizontal and trends NNW, which is nearly perpendicular to the E-striking fault. Therefore, the Gole Larghe is yet another example of a severely misoriented fault with a wide complex fault zone architecture.

This brief survey demonstrates that wide multi-cored fault zones are not limited to specific protoliths, certain ranges of cumulative displacement, nor any particular mode of slip. Quite to the contrary, Table 2 shows that wide multi-cored fault zones span the extremes of each of these parameters. The only factor that all of these global occurrences have in common is misorientation with respect to the greatest principal compressive stress, which is consistent with our findings in the Sierra Cucapah.

Strain Hardening

The relocation and redistribution of shearing that leads to the formation of multiple high-strain zones in a single fault requires some form of strain hardening (e.g., Chester and Chester, 1998; Di Toro and Pennacchioni, 2005; Cowgill et al., 2004a; Faulkner et al., 2008). Regardless of protolith, strain hardening and the development of wide multicored faults may result from the healing of gouge with compaction and fluid induced cementation, which gives rise to dilatancy strengthening (Morrow et al., 1982; Marone et al., 1990; Marone, 1998a, 1998b; Hirakawa and Ma, 2016). This hypothesis predicts that abandoned fault cores should be more strongly compacted and/or mineralized than active fault cores, but such evidence has yet to be well documented. In the Sierra Cucapah, syn-kinematic alteration is not restricted to wide complex fault zones, and relatively simple single-cored faults like the Laguna Salada fault are associated with extensive hydrothermal alteration.

Due to the expected low strength contrast of faults developed in anisotropic phyllosilicate protoliths, small changes in strength of gouge could have large effects on the localization of future increments of shearing. We propose that in such faults, cataclasis may be inherently characterized by strain hardening. Cataclasite and gouge not only have a smaller grain size, but these rocks are also likely to have a diminished grain-shape fabric (e.g., Heilbronner and Keulen, 2006) and alignment of phyllosilicate grains compared to a strongly foliated metasedimentary protolith. This should reduce the continuity of

slip surfaces defined by aligned mica and lead to a strengthening of the fault rock compared to its protolith. Collettini et al. (2009) demonstrated that powdered samples with smaller grain size and no preferred grain alignment have a twofold increase in frictional strength compared to equivalent rocks that are naturally foliated. Another effect of cataclasis is to change the rate-state frictional properties from velocity weakening of the protolith to velocity strengthening of the gouge.

We propose that the predicted strain hardening of multi-cored fault zones is associated with the one parameter that all of these examples have in common: severe misorientation and high normal stress. The difference in normal stress of two faults that form angles of 30° (optimally oriented) and 80° (severely misoriented) to the maximum compressive stress is ~72% of the applied differential stress. Yield strength, which is proportional to normal stress, may be several times greater for misoriented faults compared to optimally oriented faults. Therefore, we agree with Cowgill et al. (2004b) who proposed that the rotation of a fault relative to principal stress should result in either strain hardening or strain softening.

Our proposed genetic association of misorientation with wide multicore fault zones does not require these faults to have experienced high normal stress throughout their entire slip history. As orogenic strain accumulates by progressive general shear, a deformation path that consists of both pure and simple shear components, all planar markers progressively rotate toward the principal extension axis, which commonly is oriented at a high angle, if not perpendicular, to the regional maximum compressive stress (Fossen and Tikoff, 1993; Tikoff and Wojtal, 1999). Therefore, all faults, regardless of their initial orientation, should rotate to progressively greater angles of misorientation relative to regional stress. Likewise principal stress axes can also rotate with respect to stationary features in the crust due to a change in tectonic loading. Such a mechanism, associated with basin and range extension, may be responsible for the high angle of principal normal stress with respect to the San Andreas fault. We propose that as long as some of the cumulative slip has occurred under high normal stress, a fault may develop a wide multicore architecture. With only 1100 m of total dextral displacement (Di Toro and Pennacchioni, 2005), the Gole Larghe fault zone demonstrates an example of the lower limit of cumulative slip needed to generate a wide complex fault zone.

CONCLUSIONS

Field relationships in the Sierra Cucapah demonstrate a strong correlation between the style of faulting associated with the infinitesimal strain of a single earthquake rupture and the internal structure of the long-lived fault zone. We recognize three distinct types of faults. Type 1 faults have narrow damage zones (<100 m in width) and a single high-strain core. Coseismic slip is contained within the fault zone and highly concentrated (60%–90%) onto a single principal scarp that coincides with the fault core. Type 2 faults have wide damage zones (several hundred meters in width) with multiple overlapping high-strain cores. Coseismic slip is widely distributed on multiple (5–20) overlapping scarps that exist entirely within the fault zone. Type 3 faults also have wide damage zones with multiple cores, and additionally, they are more strongly affected by subsidiary faults, some of which cut previously formed cores and extend several kilometers beyond the limits of the damage zone. Coseismic slip is widely distributed on multiple scarps and becomes transferred to subsidiary faults that diverge and remerge with the main fault along strike. Kinematic partitioning of oblique coseismic slip is most strongly developed in type 3 faults compared to the other two classes. Even in the cases of greatest rupture complexity, all paleoscarps from earlier events were reactivated by scarp-forming faults of the most recent earthquake, which indicates high repeatability of rupture fabrics and kinematics in consecutive events.

Our work supports the widely accepted hypothesis that strain softening leads to progressive localization of slip to form simple narrow fault zones that have a single high-strain core, whereas, strain hardening leads to the redistribution of slip and the development of wide complex multi-cored fault zones. Grain-size reduction and alteration reactions increase phyllosilicate concentrations, which drives progressive weakening that localizes strain into the core of a fault. However, if the host rock is already rich in phyllosilicates, such as in the cases of metasedimentary schist and gneiss, the degree of cataclastic weakening is greatly diminished. In these cases, cataclasis itself may result in strengthening by disrupting preexisting foliations and reducing the continuity of slip surfaces in the rock. Additionally, when protolith-core strength contrast is low, the small changes associated with the velocity strengthening properties of cataclasite and gouge may be sufficient to relocate strain to less deformed areas of the fault zone that are characterized by velocity weakening.

Many fault sections in the Sierra Cucapah and throughout the world display wide multicore architecture (Table 1), but are developed in granitoid rocks, which is somewhat counterintuitive given the large expected contrast in the strength of protolith and core. However, all such examples presented in this study correspond to faults that are severely misoriented with respect to the greatest principal normal stress. Therefore, regardless of the physical properties of the gouge and cataclasite that they contain, the cores of these faults must be greatly strengthened by high magnitudes of the applied normal stress.

It stands to reason that wear and damage should increase with the amount of cumulative slip accommodated across a fault, but several factors work to inhibit the existence of a straight forward relationship. The rate of gouge production decreases significantly with progressive deformation as fracture energy from slip events further reduces grain size of pre-existing gouge without adding appreciably to its volume (Yoshioka, 1986). Therefore, faults that undergo progressive weakening should produce less gouge and wear than those that experience progressive strengthening. This suggests that orientation-controlled variations in the applied normal stress and protolith-core strength contrasts are essential to consider when assessing the role of cumulative slip on fault zone architecture.

ACKNOWLEDGMENTS

This work was financed by Consejo Nacional de Ciencia y Tecnología, Mexico City, Mexico (CB-2014-239818) and the Southern California Earthquake Center (SCEC), Los Angeles, California, USA (EAR-1033462 and U.S. Geological Survey G12AC20038, SCEC paper 10004). The paper was greatly improved by reviews from Victoria Langenheim, Deven McPhillips, Jaime Delano, Michael Taylor, and An Yin. We are grateful for technical support provided by Jose Mojarro and Luis Gradilla. We also thank Jaime Delano and other reviewers for their suggestions and comments that greatly improved the paper.

REFERENCES CITED

Axen, G.J., 1992, Pore pressure, stress increase, and fault weakening in low-angle normal faulting: Journal of Geophysical Research. Solid Earth, v. 97, p. 8979–8991, https://doi.org/10.1029/92JB00517.

Axen, G.J., 2004, Mechanics of low-angle normal faults, *in* Karner, G.D., Taylor, B., Driscoll, N., and Kohlsted, D.L., eds., Rheology and Deformation of the Lithosphere at Continental Margins: New York, USA, Columbia University Press, p. 46–91, https://cup.columbia.edu/book/rheology-and-deformation-of-the-lithosphere-at-continental-margins/9780231127394.

Axen, G.J., and Fletcher, J.M., 1998, Late Miocene-Pleistocene extensional faulting, Northern Gulf of California, Mexico and Salton Trough, California: International Geology Review, v. 40, p. 217–244, https://doi.org/10.1080/00206819809465207.

Axen, G.J., Fletcher, J.M., Cowgill, E., Murphy, M.A., Kapp, P., MacMillan, I., Ramos-Velázquez, E., and Aranda-Gómez, J.J., 1999, Range-front fault scarps of the Sierra El Mayor, Baja California: Formed above an active low-angle normal fault?: Geology, v. 27, p. 247–250, https://doi.org/10.1130/0091-7613(1999)027<0247:RFFSOT>2.3.CO;2.

Axen, G.J., Stockli, D.F., Grove, M., Lovera, O.M., Rothstein, D.A., Fletcher, J.M., and Farley, K.A., 2000, Thermal evolution of Monte Blanco dome: Low-angle normal faulting during Gulf of California rifting and late Eocene denudation of the eastern Peninsular Ranges: Tectonics, v. 19, p. 197–212, https://doi.org/10.1029/1999TC001123.

Barnard, F.L., 1968, Structural geology of the Sierra de los Cucapas, northeastern Baja California, Mexico, and Imperial County, California [Ph.D. thesis]: Boulder, Colorado, USA, University of Colorado, 157 p.

Barrows, A.G., Kahle, J.E., and Beeby, D.J., 1985, Earthquake Hazards and Tectonic History of the San Andreas Fault Zone, Los Angeles County, California: California Department of Conservation, Division of Mines and Geology Open-File Report 85-10, 236 p., 21 plates, scale 1:12,000.

Ben-Zion, Y., and Sammis, C.G., 2003, Characterization of fault zones: Pure and Applied Geophysics, v. 160, p. 677–715, https://doi.org/10.1007/PL00012554.

Biegel, R.L., and Sammis, C.G., 2004, Relating fault mechanics to fault zone structure: Advances in Geophysics, v. 47, p. 65–111, https://doi.org/10.1016/S0065-2687(04)47002-2.

Bott, M.H.P., 1959, The mechanics of oblique slip faulting: Geological Magazine, v. 96, p. 109–117, https://doi.org/10.1017/S0016756800059987.

Bradbury, K.K., Evans, J.P., Chester, J.S., Chester, F.M., and Kirschner, D.L., 2011, Lithology and internal structure of the San Andreas fault at depth based on characterization of Phase 3 whole-rock core in the San Andreas Fault Observatory at Depth (SAFOD) borehole: Earth and Planetary Science Letters, v. 310, p. 131–144, https://doi.org/10.1016/j.epsl.2011.07.020.

Butler, C.A., Holdsworth, R.E., and Strachan, R.A., 1995, Evidence for Caledonian sinistral strike-slip motion and associated fault zone weakening, Outer Hebrides Fault Zone, NW Scotland: Journal of the Geological Society, v. 152, p. 743–746, https://doi.org/10.1144/gsjgs.152.5.0743.

Byerlee, J.D., 1978, Friction of rocks: Pure and Applied Geophysics, v. 116, p. 615–626, https://doi.org/10.1007/BF00876528.

Caine, J.S., Evans, J.P., and Forster, C.B., 1996, Fault zone architecture and permeability structure: Geology, v. 24, p. 1025–1028, https://doi.org/10.1130/0091-7613(1996)024<1025:FZAAPS>2.3.CO;2.

Carpenter, B.M., Marone, C., and Saffer, D.M., 2011, Weakness of the San Andreas Fault revealed by samples from the active fault zone: Nature Geoscience, v. 4, p. 251–254, https://doi.org/10.1038/ngeo1089.

Caskey, S.J., Wesnousky, S.G., Zhang, P., and Slemmons, D.B., 1996, Surface faulting of the 1954 Fairview Peak (MS 7.2) and Dixie Valley (MS 6.8) earthquakes, central Nevada: Bulletin of the Seismological Society of America, v. 86, p. 761–787.

Chanes-Martínez, J.J., González-Escobar, M., Suárez-Vidal, F., and Gallardo-Mata, C.G., 2014, Structural geometry of a sector of the Colorado river delta, Baja California, Mexico, based on seismic reflections: Pure and Applied Geophysics, v. 171, p. 1107–1127, https://doi.org/10.1007/s00024-013-0729-z.

Chester, F.M., and Chester, J.S., 1998, Ultracataclasite structure and friction processes of the Punchbowl fault, San Andreas system, California: Tectonophysics, v. 295, p. 199–221, https://doi.org/10.1016/S0040-1951(98)00121-8.

Chester, F.M., and Logan, J.M., 1986, Implications for mechanical properties of brittle faults from observations of the Punchbowl fault zone, California: Pure and Applied Geophysics, v. 124, p. 79–106, https://doi.org/10.1007/BF00875720.

Chester, F.M., Evans, J.P., and Biegel, R.L., 1993, Internal structure and weakening mechanisms of the San Andreas Fault: Journal of Geophysical Research. Solid Earth, v. 98, p. 771–786, https://doi.org/10.1029/92JB01866.

Chora-Salvador, J.M., 2003, Analisis cinematico de fallas neogenicas normales de alto y bajo angulo en la Sierra Cucapa, Baja California, Mexico: Centro de Investigación Científica y de Educación Superior de Ensenada, 1 p.

Collettini, C., and Sibson, R.H., 2001, Normal faults, normal friction?: Geology, v. 29, p. 927–930, https://doi.org/10.1130/0091-7613(2001)029<0927:NFNF>2.0.CO;2.

Collettini, C., Niemeijer, A.R., Viti, C., and Marone, C., 2009, Fault zone fabric and fault weakness: Nature, v. 462, p. 907–910, https://doi.org/10.1038/nature08585.

Cowgill, E., Arrowsmith, J.R., Yin, A., Xiaofeng, W., and Zhengle, C., 2004a, The Akato Tagh bend along the Altyn Tagh fault, northwest Tibet 2: Active deformation and the importance of transpression and strain hardening within the Altyn Tagh system: Geological Society of America Bulletin, v. 116, p. 1443–1464, https://doi.org/10.1130/B25360.1.

Cowgill, E., Yin, A., Arrowsmith, J.R., Feng, W.X., and Shuanhong, Z., 2004b, The Akato Tagh bend along the Altyn Tagh fault, northwest Tibet 1: Smoothing by vertical-axis rotation and the effect of topographic stresses on bend-flanking faults: Geological Society of America Bulletin, v. 116, p. 1423–1442, https://doi.org/10.1130/B25359.1.

Di Toro, G., and Pennacchioni, G., 2005, Fault plane processes and mesoscopic structure of a strong-type seismogenic fault in tonalites (Adamello batholith, Southern Alps): Tectonophysics, v. 402, p. 55–80, https://doi.org/10.1016/j.tecto.2004.12.036.

Donath, F.A., 1961, Experimental study of shear failure in anisotropic rocks: Geological Society of America Bulletin, v. 72, p. 985–989, https://doi.org/10.1130/0016-7606(1961)72[985:ESOSFI]2.0.CO;2.

Dor, O., Rockwell, T.K., and Ben-Zion, Y., 2006, Geological observations of damage asymmetry in the structure of the San Jacinto, San Andreas and Punchbowl faults in southern California: A possible indicator for preferred rupture propagation direction: Pure and Applied Geophysics, v. 163, p. 301–349, https://doi.org/10.1007/s00024-005-0023-9.

Dorsey, R.J., and Martin-Barajas, A., 1999, Sedimentation and deformation in a Pliocene-Pleistocene transtensional supradetachment basin, Laguna Salada, northwest Mexico: Basin Research, v. 11, p. 205–221, https://doi.org/10.1046/j.1365-2117.1999.00096.x.

Dorsey, M.T., Rockwell, T.K., Girty, G.H., Ostermeijer, G., Mitchell, T.M., and Fletcher, J.M., 2017, Evidence of Na- and Mg-rich hydrothermal brines driving chloritization and albitization in an active fault zone: Case study of the Borrego fault, Baja CA, Mexico: presented at the Southern California Earthquake Center Annual Meeting, 15 August, no. 7839.

Faulkner, D.R., Lewis, A.C., and Rutter, E.H., 2003, On the internal structure and mechanics of large strike-slip fault zones: Field observations of the Carboneras fault in southeastern Spain: Tectonophysics, v. 367, p. 235–251, https://doi.org/10.1016/S0040-1951(03)00134-3.

Faulkner, D.R., Mitchell, T.M., Healy, D., and Heap, M.J., 2006, Slip on "weak" faults by the rotation of regional stress in the fracture damage zone: Nature, v. 444, p. 922–925, https://doi.org/10.1038/nature05353.

Faulkner, D.R., Mitchell, T.M., Rutter, E.H., and Cembrano, J., 2008, On the structure and mechanical properties of large strike-slip faults, *in* Wibberley, C.A.J., Kurz, W., Imber, J., Holdsworth, R.E., and Collettini, C., eds., The Internal Structure of Fault Zones: Fluid Flow and Mechanical Properties: Geological Society, London, Special Publication 299, p. 139–150, https://doi.org/10.1144/SP299.9.

Faulkner, D.R., Jackson, C.A.L., Lunn, R.J., Schlische, R.W., Shipton, Z.K., Wibberley, C.A.J., and Withjack, M.O., 2010, A review of recent developments concerning the structure, mechanics and fluid flow properties of fault zones: Journal of Structural Geology, v. 32, p. 1557–1575, https://doi.org/10.1016/j.jsg.2010.06.009.

Fletcher, J.M., and Spelz, R.M., 2009, Patterns of Quaternary deformation and rupture propagation associated with an active low-angle normal fault, Laguna Salada, Mexico: Evidence of a rolling hinge?: Geosphere, v. 5, p. 385–407, https://doi.org/10.1130/GES00206.1.

Fletcher, J.M., Oskin, M.E., and Teran, O.J., 2016, The role of a keystone fault in triggering the complex El Mayor–Cucapah earthquake rupture: Nature Geoscience, v. 9, p. 303–307, https://doi.org/10.1038/ngeo2660.

Fletcher, J.M., Teran, O.J., Rockwell, T.K., Oskin, M.E., Hudnut, K.W., Mueller, K.J., Spelz, R.M., Akciz, S.O., Masana, E., Faneros, P.G., Fielding, E.J., Leprince, P.S., Morelan, A.E., Stock, J.M., Lynch, D.K., Elliott, A.J., Gold, P., Liu-Zeng, J., González-Ortega, A., Hinojosa-Corona, A., and González-García, J., 2014, Assembly of a large earthquake from a complex fault system: Surface rupture kinematics of the 4 April 2010 El Mayor–Cucapah (Mexico) M_w 7.2 earthquake: Geosphere, v. 10, p. 797–827, https://doi.org/10.1130/GES00933.1.

Fossen, H., and Tikoff, B., 1993, The deformation matrix for simultaneous simple shearing, pure shearing and volume change, and its application to transpression-transtension tectonics: Journal of Structural Geology, v. 15, p. 413–422, https://doi.org/10.1016/0191-8141(93)90137-Y.

Fossen, H., Tikoff, B., and Teyssier, C., 1994, Strain modeling of transpressional and transtensional deformation: Norsk Geologisk Tidskrift, v. 74, p. 134–145.

Frost, E., Dolan, J.F., Sammis, C.G., Hacker, B., Cole, J., and Ratschbacher, L., 2009, Progressive strain localization in a major strike-slip fault exhumed from midseismogenic depths: Structural observations from the Salzach-Ennstal-Mariazell-Puchberg fault system, Austria: Journal of Geophysical Research. Solid Earth, v. 114, https://doi.org/10.1029/2008JB005763.

García-Abdeslem, J., Espinosa-Cardeña, J.M., Munguía-Orozco, L., Wong-Ortega, V.M., and Ramírez-Hernández, J.J., 2001, Crustal structure from 2-D gravity and magnetic data modeling, magnetic power spectrum inversion, and seismotectonics in the Laguna Salada basin, northern Baja California, Mexico: Geofísica Internacional, v. 40, p. 67–85.

Hayman, N.W., Knott, J.R., Cowan, D.S., Nemser, E.S., and Sarna-Wojcicki, A.M., 2003, Quaternary low-angle slip on detachment faults in Death Valley, California: Geology, v. 31, p. 343–346, https://doi.org/10.1130/0091-7613(2003)031<0343:QLASOD>2.0.CO;2.

Heidbach, O., Tingay, M., Barth, A., Reinecker, J., Kurfess, D., and Muller, B., 2009, World Stress Map: Potsdam, Germany, German Research Centre for Geosciences, https://doi.org/10.1594/GFZ.WSM.Map2009.

Heilbronner, R., and Keulen, N., 2006, Grain size and grain shape analysis of fault rocks: Tectonophysics, v. 427, p. 199–216, https://doi.org/10.1016/j.tecto.2006.05.020.

Hernandez Flores, A.P., 2015, Paleosismología del sistema de fallas imbricado en la Sierra Cucapah, Baja California, México: Centro de Investigación Científica y de Educación Superior de Ensenada, 1 p.

Hernandez Flores, A.P., Fletcher, J.M., Spelz, R.M., Rockwell, T.K., and Teran, O.J., 2013, Paleoseismology of the imbricate fault array in the Sierra Cucapah, northern Baja California, Mexico: Abstract 1668977 presented at American Geophysical Union Meeting of the Americas, Cancun, Mexico, 14–17 May.

Hirakawa, E., and Ma, S., 2016, Dynamic fault weakening and strengthening by gouge compaction and dilatancy in a fluid-saturated fault zone: Journal of Geophysical Research. Solid Earth, v. 121, p. 5988–6008, https://doi.org/10.1002/2015JB012509.

Hull, J., 1988, Thickness-displacement relationships for deformation zones: Journal of Structural Geology, v. 10, p. 431–435, https://doi.org/10.1016/0191-8141(88)90020-X.

Ikari, M.J., Saffer, D.M., and Marone, C., 2009, Frictional and hydrologic properties of clay-rich fault gouge: Journal of Geophysical Research. Solid Earth, v. 114, https://doi.org/10.1029/2008JB006089.

Karner, S.L., Marone, C., and Evans, B., 1997, Laboratory study of fault healing and lithification in simulated fault gouge under hydrothermal conditions: Tectonophysics, v. 277, p. 41–55, https://doi.org/10.1016/S0040-1951(97)00077-2.

Kelm, L.D., 1971, A gravity and magnetic study of the Laguna Salada area, Baja California, Mexico [M.Sc. thesis]: San Diego, California, USA, San Diego State College, 103 p.

Lockner, D.A., Morrow, C.A., Moore, D.E., and Hickman, S.H., 2011, Low strength of deep San Andreas fault gouge from SAFOD core: Nature, v. 472, p. 82–85, https://doi.org/10.1038/nature09927.

Marone, C., 1998a, Laboratory-derived friction laws and their application to seismic faulting: Annual Review of Earth and Planetary Sciences, v. 26, p. 643–696, https://doi.org/10.1146/annurev.earth.26.1.643.

Marone, C., 1998b, The effect of loading rate on static friction and the rate of fault healing during the earthquake cycle: Nature, v. 391, p. 69–72, https://doi.org/10.1038/34157.

Marone, C., Raleigh, C.B., and Scholz, C.H., 1990, Frictional behavior and constitutive modeling of simulated fault gouge: Journal of Geophysical Research. Solid

Earth, v. 95, p. 7007–7025, https://doi.org/10.1029/JB095iB05p07007.
Matthews, V., III, 1976, Correlation of the Pinnacles and Neenach volcanic formations and their bearing on the San Andreas fault problem: American Association of Petroleum Geologists Bulletin, v. 60, p. 2128–2141.
Melosh, H.J., 1990, Mechanical basis for low-angle normal faulting in the Basin and Range Province: Nature, v. 343, p. 331–335, https://doi.org/10.1038/343331a0.
Mitchell, T.M., and Faulkner, D.R., 2009, The nature and origin of off-fault damage surrounding strike-slip fault zones with a wide range of displacements: A field study from the Atacama fault system, northern Chile: Journal of Structural Geology, v. 31, p. 802–816, https://doi.org/10.1016/j.jsg.2009.05.002.
Moore, D.E., and Lockner, D.A., 2007, Friction of the smectite clay montmorillonite: A review and interpretation of data, *in* Dixon, T.H., and Moore, J.C., eds., The Seismogenic Zone of Subduction Thrust Faults: New York, USA, Columbia University Press, p. 317–345, http://cup.columbia.edu/book/the-seismogenic-zone-of-subduction-thrust-faults/9780231138666.
Moore, D.E., and Rymer, M.J., 2007, Talc-bearing serpentinite and the creeping section of the San Andreas fault: Nature, v. 448, p. 795–797, https://doi.org/10.1038/nature06064.
Moore, D.E., and Rymer, M.J., 2012, Correlation of clayey gouge in a surface exposure of serpentinite in the San Andreas Fault with gouge from the San Andreas Fault Observatory at Depth (SAFOD): Journal of Structural Geology, v. 38, p. 51–60, https://doi.org/10.1016/j.jsg.2011.11.014.
Morris, A.P., Ferrill, D.A., and Brent Henderson, D.B., 1996, Slip-tendency analysis and fault reactivation: Geology, v. 24, p. 275–278, https://doi.org/10.1130/0091-7613(1996)024<0275:STAAFR>2.3.CO;2.
Morrow, C.A., Shi, L.Q., and Byerlee, J.D., 1982, Strain hardening and strength of clay-rich fault gouges: Journal of Geophysical Research. Solid Earth, v. 87, p. 6771–6780, https://doi.org/10.1029/JB087iB08p06771.
Morton, N., Girty, G.H., and Rockwell, T.K., 2012, Fault zone architecture of the San Jacinto fault zone in Horse Canyon, southern California: A model for focused post-seismic fluid flow and heat transfer in the shallow crust: Earth and Planetary Science Letters, v. 329–330, p. 71–83, https://doi.org/10.1016/j.epsl.2012.02.013.
Mueller, K.J., and Rockwell, T.K., 1991, Late Quaternary structural evolution of the western margin of the Sierra Cucapa, northern Baja California: Chapter 14: Part III. Regional geophysics and geology, *in* Dauphin, J.P., and Simoneit, B.R.T., eds., The Gulf and Peninsular Province of the Californias: Tulsa, Oklahoma, American Association of Petroleum Geologists Memoir 47, p. 249–260.
Mueller, K.J., and Rockwell, T.K., 1995, Late Quaternary activity of the Laguna Salada Fault in northern Baja California, Mexico: Geological Society of America Bulletin, v. 107, p. 8–18, https://doi.org/10.1130/0016-7606(1995)107<0008:LQAOTL>2.3.CO;2.
Nieto-Samaniego, A.F., 1999, Stress, strain and fault arrays: Journal of Structural Geology, v. 21, p. 1065–1070, https://doi.org/10.1016/S0191-8141(99)00016-4.
Nieto-Samaniego, A.F., and Alaniz-Alvarez, S.A., 1995, Influence of the structural framework on the origin of multiple fault patterns: Journal of Structural Geology, v. 17, p. 1571–1577, https://doi.org/10.1016/0191-8141(95)00048-I.
Nieto-Samaniego, A.F., and Alaniz-Alvarez, S.A., 1997, Origin and structural interpretation of multiple fault patterns: Tectonophysics, v. 270, p. 197–206, https://doi.org/10.1016/S0040-1951(96)00216-8.
Numelin, T., Marone, C., and Kirby, E., 2007, Frictional properties of natural fault gouge from a low-angle normal fault, Panamint Valley, California: Tectonics, v. 26, https://doi.org/10.1029/2005TC001916.
Oskin, M.E., Arrowsmith, J.R., Corona, A.H., Elliott, A.J., Fletcher, J.M., Fielding, E.J., Gold, P.O., Gonzalez-Garcia, J.J., Hudnut, K.W., and Liu-Zeng, J., 2012, Near-field deformation from the El Mayor–Cucapah earthquake revealed by differential LIDAR: Science, v. 335, p. 702–705, https://doi.org/10.1126/science.1213778.
Powell, R.E., 1993, Balanced palinspastic reconstruction of pre-late Cenozoic paleogeology, southern California: Geologic and kinematic constraints on evolution of the San Andreas fault system, *in* Powell, R.E., Weldon, R.J., II, and Matti, J.C., eds., The San Andreas Fault System: Displacement, Palinspastic Reconstruction, and Geologic Evolution, Geological Society of America Memoir 178, p. 1–6, https://doi.org/10.1130/MEM178-p1.
Rempe, M., Mitchell, T., Renner, J., Nippress, S., Ben-Zion, Y., and Rockwell, T.K., 2013, Damage and seismic velocity structure of pulverized rocks near the San Andreas Fault: Journal of Geophysical Research. Solid Earth, v. 118, p. 2813–2831, https://doi.org/10.1002/jgrb.50184.
Rice, J.R., 1992, Fault stress states, pore pressure distributions, and the weakness of the San Andreas fault, *in* Evans, B., and Wong, T.-F., eds., Fault Mechanics and Transport Properties of Rocks: San Diego, California, USA, Academic Press, p. 475–503, https://doi.org/10.1016/S0074-6142(08)62835-1.
Rockwell, T.K., and Ben-Zion, Y., 2007, High localization of primary slip zones in large earthquakes from paleoseismic trenches: Observations and implications for earthquake physics: Journal of Geophysical Research. Solid Earth, v. 112, https://doi.org/10.1029/2006jb004764.
Rockwell, T.K., Sisk, M., Girty, G.H., Dor, O., Wechsler, N., and Ben-Zion, Y., 2009, Chemical and physical characteristics of pulverized Tejon Lookout granite adjacent to the San Andreas and Garlock faults: Implications for earthquake physics: Pure and Applied Geophysics, v. 166, p. 1725–1746, https://doi.org/10.1007/s00024-009-0514-1.
Rubin, A.M., Gillard, D., and Got, J.-L., 1999, Streaks of microearthquakes along creeping faults: Nature, v. 400, p. 635–641, https://doi.org/10.1038/23196.
Rymer, M.J., Hickman, S.H., and Stoffer, P.W., 2006, A field guide to the central, creeping section of the San Andreas Fault and the San Andreas Fault Observatory at Depth, *in* Prentice, C.S., Scotchmoor, J.G., Moores, E.M., and Kiland, J.P., eds., 1906 San Francisco Earthquake Centennial Field Guides: Field Trips Associated with the 100th Anniversary Conference, 18–23 April, San Francisco, California: Geological Society of America Field Guide 7, p. 237–272.
Saffer, D.M., and Marone, C., 2003, Comparison of smectite- and illite-rich gouge frictional properties: Application to the updip limit of the seismogenic zone along subduction megathrusts: Earth and Planetary Science Letters, v. 215, p. 219–235, https://doi.org/10.1016/S0012-821X(03)00424-2.
Scholz, C.H., 1987, Wear and gouge formation in brittle faulting: Geology, v. 15, p. 493, https://doi.org/10.1130/0091-7613(1987)15<493:WAGFIB>2.0.CO;2.
Shipton, Z.K., and Cowie, P.A., 2001, Damage zone and slip-surface evolution over μm to km scales in high-porosity Navajo sandstone, Utah: Journal of Structural Geology, v. 23, p. 1825–1844, https://doi.org/10.1016/S0191-8141(01)00035-9.
Sibson, R.H., 1977, Fault rocks and fault mechanisms: Journal of the Geological Society, v. 133, p. 191–213, https://doi.org/10.1144/gsjgs.133.3.0191.
Sieh, K.E., 1978, Slip along the San Andreas fault associated with the great 1857 earthquake: Bulletin of the Seismological Society of America, v. 68, p. 1421–1448.
Siem, M.E., 1992, The structure and petrology of Sierra El Mayor, northeastern Baja California, Mexico: San Diego State University, 1 p., https://digitallibrary.sdsu.edu/islandora/object/sdsu%3A193.
Smith, S.A.F., Bistacchi, A., Mitchell, T.M., Mittempergher, S., and Di Toro, G., 2013, The structure of an exhumed intraplate seismogenic fault in crystalline basement: Tectonophysics, v. 599, p. 29–44, https://doi.org/10.1016/j.tecto.2013.03.031.
Spelz, R.M., Fletcher, J.M., Owen, L.A., and Caffee, M.W., 2008, Quaternary alluvial-fan development, climate and morphologic dating of fault scarps in Laguna Salada, Baja California, Mexico: Geomorphology, v. 102, p. 578–594, https://doi.org/10.1016/j.geomorph.2008.06.001.
Stapel, G., Moeys, R., and Biermann, C., 1996, Neogene evolution of the Sorbas basin (SE Spain) determined by paleostress analysis: Tectonophysics, v. 255, p. 291–305, https://doi.org/10.1016/0040-1951(95)00190-5.
Teran, O.J., Fletcher, J.M., Oskin, M.E., Rockwell, T.K., Hudnut, K.W., Spelz, R.M., Akciz, S.O., Hernandez Flores, A.P., and Morelan, A.E., 2015, Geologic and structural controls on rupture zone fabric: A field-based study of the 2010 Mw 7.2 El Mayor-Cucapah earthquake surface rupture: Geosphere, v. 11, p. 899–920, https://doi.org/10.1130/GES01078.1.
Tikoff, B., and Wojtal, S.F., 1999, Displacement control of geologic structures: Journal of Structural Geology, v. 21, p. 959–967, https://doi.org/10.1016/S0191-8141(99)00045-0.
Tong, H., and Yin, A., 2011, Reactivation tendency analysis: A theory for predicting the temporal evolution of preexisting weakness under uniform stress state: Tectonophysics, v. 503, p. 195–200, https://doi.org/10.1016/j.tecto.2011.02.012.
Wallace, R.E., 1951, Geometry of shearing stress and relation to faulting: The Journal of Geology, v. 59, p. 118–130, https://doi.org/10.1086/625831.
Wei, S., Fielding, E.J., Leprince, P.S., Sladen, A., Avouac, J.P., Helmberger, D.V., Hauksson, E., Chu, R., Simons, M., and Hudnut, K.W., 2011, Superficial simplicity of the 2010 El Mayor-Cucapah earthquake of Baja California in Mexico: Nature Geoscience, v. 4, p. 615–618, https://doi.org/10.1038/ngeo1213.
Wesnousky, S.G., and Jones, C.H., 1994, Oblique slip, slip partitioning, spatial and temporal changes in the regional stress field, and the relative strength of active faults in the Basin and Range, western United States: Geology, v. 22, p. 1031, https://doi.org/10.1130/0091-7613(1994)022<1031:OSSPSA>2.3.CO;2.
Wibberley, C.A.J., Yielding, G., and Di Toro, G., 2008, Recent advances in the understanding of fault zone internal structure: A review, *in* Wibberley, C.A.J., Imber, J., Holdsworth, R.E., Collettini, C., and Kurz, W., eds., The Internal Structure of Fault Zones: Fluid Flow and Mechanical Properties: Geological Society, London, Special Publication 299, p. 5–33, https://doi.org/10.1144/SP299.2.
Yan, Y., van der Pluijm, B.A., and Peacor, D.R., 2001, Deformation microfabrics of clay gouge, Lewis Thrust, Canada: A case for fault weakening from clay transformation, *in* Holdsworth, R.E., Strachan, R.A., Magloughlin, J.F., and Knipe, R.J., eds., The Nature and Tectonic Significance of Fault Zone Weakening: Geological Society, London, Special Publication 186, p. 103–112, https://doi.org/10.1144/gsl.sp.2001.186.01.07.
Yang, W., and Hauksson, E., 2013, The tectonic crustal stress field and style of faulting along the Pacific North America Plate boundary in southern California: Geophysical Journal International, v. 194, p. 100–117, https://doi.org/10.1093/gji/ggt113.
Yin, A., 1989, Origin of regional, rooted low-angle normal faults: A mechanical model and its tectonic implications: Tectonics, v. 8, p. 469–482, https://doi.org/10.1029/TC008i003p00469.
Yoshioka, N., 1986, Fracture energy and the variation of gouge and surface roughness during frictional sliding of rocks: Journal of Physics of the Earth, v. 34, p. 335–355, https://doi.org/10.4294/jpe1952.34.335.
Zielke, O., Arrowsmith, J.R., Ludwig, L.G., and Akciz, S.O., 2010, Slip in the 1857 and earlier large earthquakes along the Carrizo Plain, San Andreas fault: Science, v. 327, p. 1119–1122, https://doi.org/10.1126/science.1182781.
Zoback, M.D., Zoback, M.L., Mount, V.S., Suppe, J., Eaton, J.P., Healy, J.H., Oppenheimer, D., Reasenberg, P.A., Jones, L., Raleigh, C.B., Wong, I.G., Scotti, O., and Wentworth, C., 1987, New evidence on the state of stress of the San Andreas fault system: Science, v. 238, p. 1105–1111, https://doi.org/10.1126/science.238.4830.1105.

Science Editor: Rob Strachan
Associate Editor: An Yin

Manuscript Received 30 March 2019
Revised Manuscript Received 6 December 2019
Manuscript Accepted 22 December 2019

Printed in the USA